Supplement of Atmos. Chem. Phys., 16, 14825–14842, 2016
http://www.atmos-chem-phys.net/16/14825/2016/
doi:10.5194/acp-16-14825-2016-supplement

Atmospheric Chemistry and Physics
Open Access
EGU

Supplement of

Temporal variability and sources of VOCs in urban areas of the eastern Mediterranean

Christos Kaltsonoudis et al.

Correspondence to: Spyros N. Pandis (spyros@chemeng.upatras.gr)

1. Measured m/z values by the PTR-MS

Table S1. Compounds measured with the PTR-MS

m/z	Target molecules	Calibration
42	Acetonitrile[2,3,4,7,8,9,10]	Acetonitrile
43	Multiple species[3,5,8,9]	*
47	Formic acid[5,8,9], Ethanol[1,9]	*
59	Acetone[1-10], propanal[10], 2,3 butanedione[10], methylvinylether[5]	Acetone
61	Acetic acid[1,3,4,5,8,9,10], Glycolaldehyde[5,10]	*
69	Isoprene[1,3,4,5,8,10], Furan[5,8,10], Other species[2,10]	Isoprene
71	MVK&MACR[2,3,4,6,8,9,10], Crotonaldehyde[10], Other species[3,10]	MVK
73	MEK[1,2,4,9,10], Methyl propanal[10], Other species[3]	MEK
75	Hydroxyl acetone[5,8,10], Methyl acetate[10], Butanol[9]	*
77	PAN[4,7,8]	*
79	Benzene[1-10], Ethyl benzene[10]	Benzene
81	Monoterpene fragments[6,8,9], Hexanal[8]	*
85	Ethyl vinyl ketone[2,8], Other species[3]	*
87	Methyl-3-butene-2-ol[6,8,9], Other species[8,10]	*
93	Toluene[1,2,3,4,8,9,10]	Toluene
95	2 vinyl furan[8,10], Phenol[5,8,9,10]	*
99	Hexanal[2,8,9]	*
101	Isoprene hyperoxides[8], Hexanal[9]	*
105	Styrene[3,8], Peroxy isobutyryl nitrate[8], Other species[6]	*
107	Xylenes[1,2,3,4,8,9,10], Ethyl benzene[4,8,10], Benzaldehyde[4,8]	Xylene
113	Various species[6]	Chlorobenzene
115	Heptanal[2,8], C7 ketones[3]	*
121	C9 aromatics[1,2,3,4,8,10]	*
129	Octanal[2,8], Naphtalene[3,8]	*
135	C10 aromatics[1,3,5]	*
137	Monoterpenes[1,4,6,8,9,]	a-pinene
139	Nopinone[6,8]	*
151	Pinonaldehyde[6,8]	*
163	C12 aromatics[3,8], Other species[6]	*

*Concentrations calculated for $k=2.0\times10^{-9}cm^3s^{-1}$

1. Lindinger et al. (1998), 2. Karl et al. (2001), 3. Karl et al. (2003), 4. DeGouw et al. (2003), 5. Christian et al. (2004), 6. Holzinger et al. (2005a), 7. Holzinger et al. (2005b), 8. DeGouw and Warneke (2007), 9. Rinne et al. (2005) ,10. Karl et al. (2007).

2. Patras summer campaign

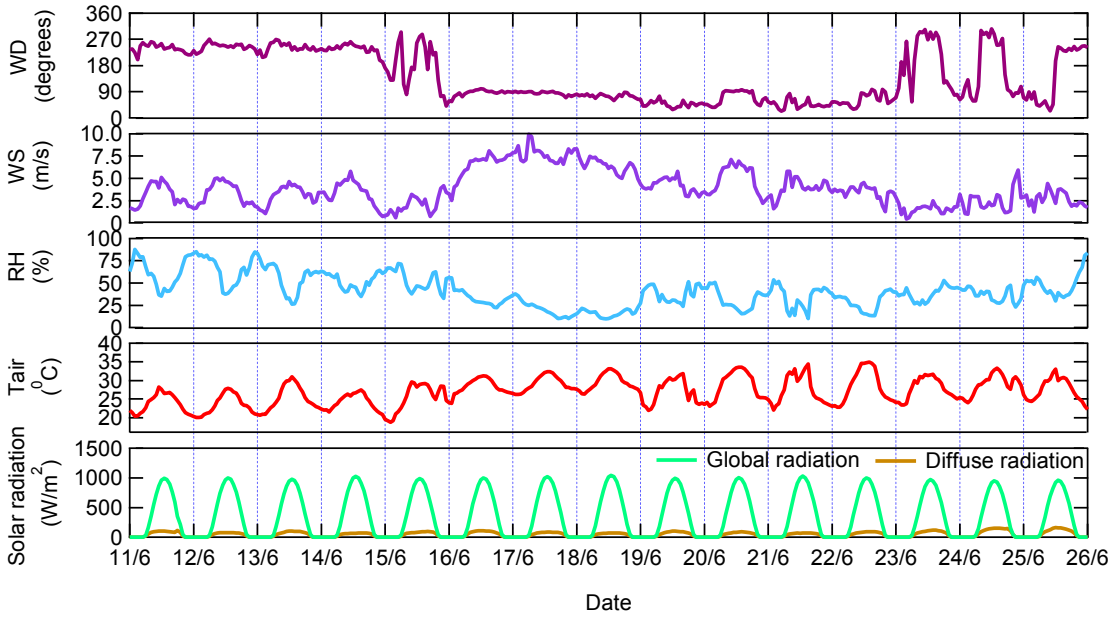

Figure S1. Meteorological conditions during the Patras summer campaign (hourly averages).

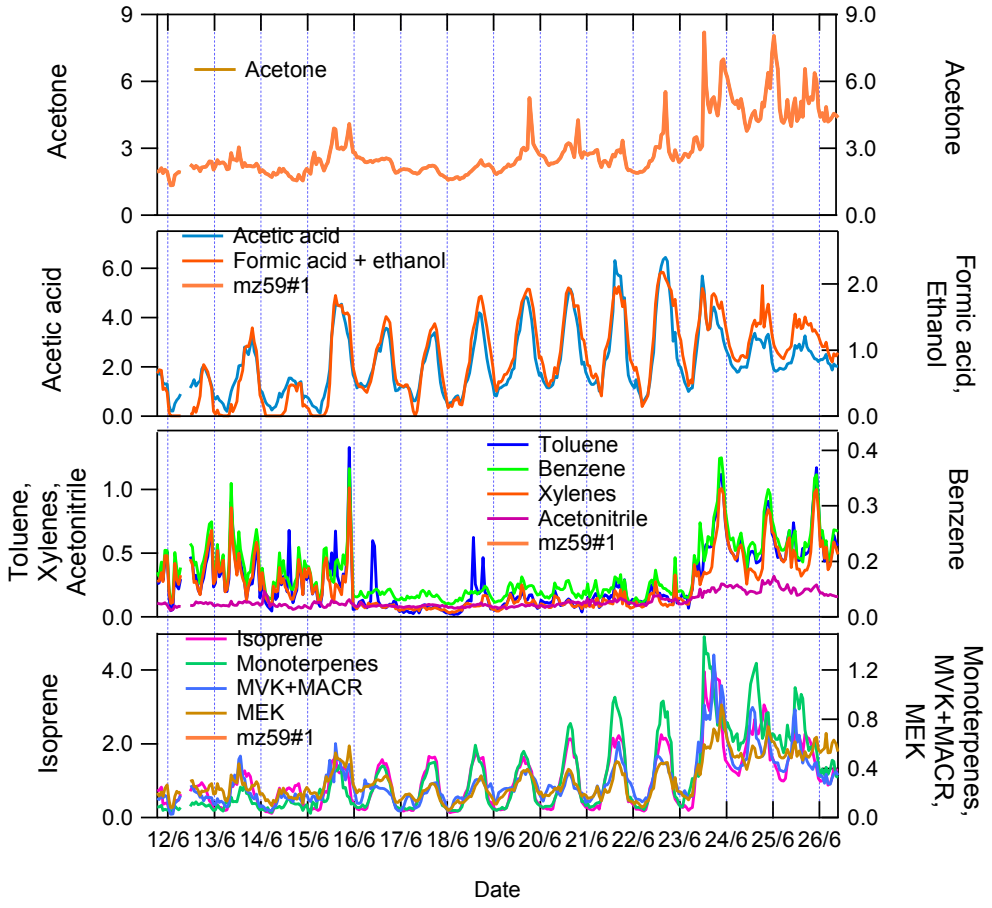

Figure S2. VOC time series for the Patras summer campaign (hourly averages). All values are in ppb.

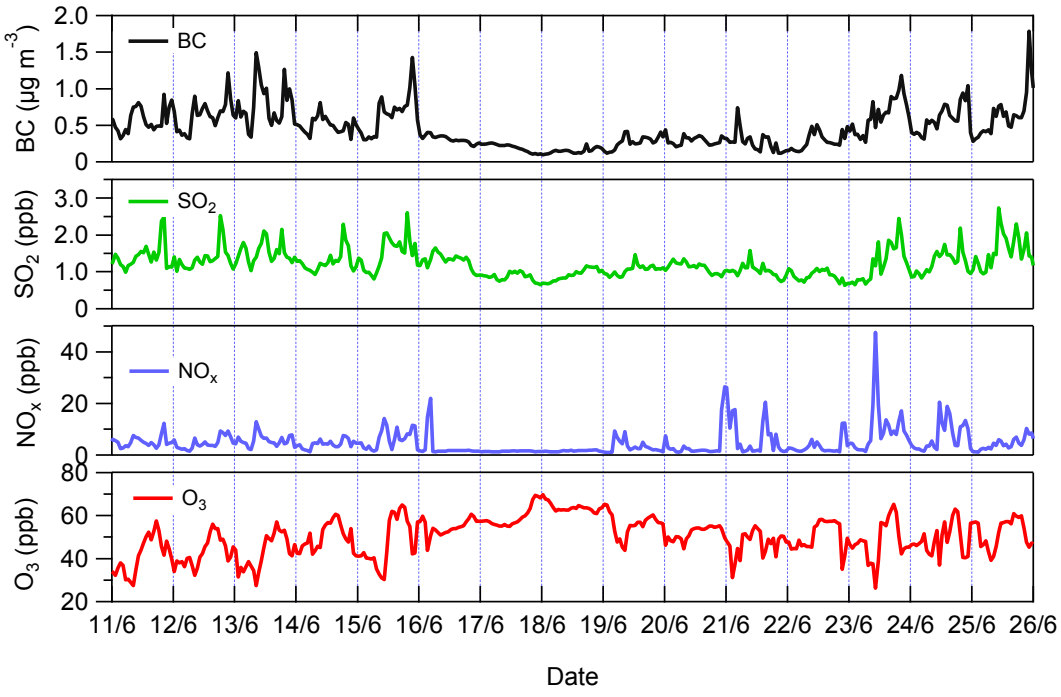

Figure S3. O_3 , NO_x, SO_2 and BC time series for the Patras summer campaign (hourly averages).

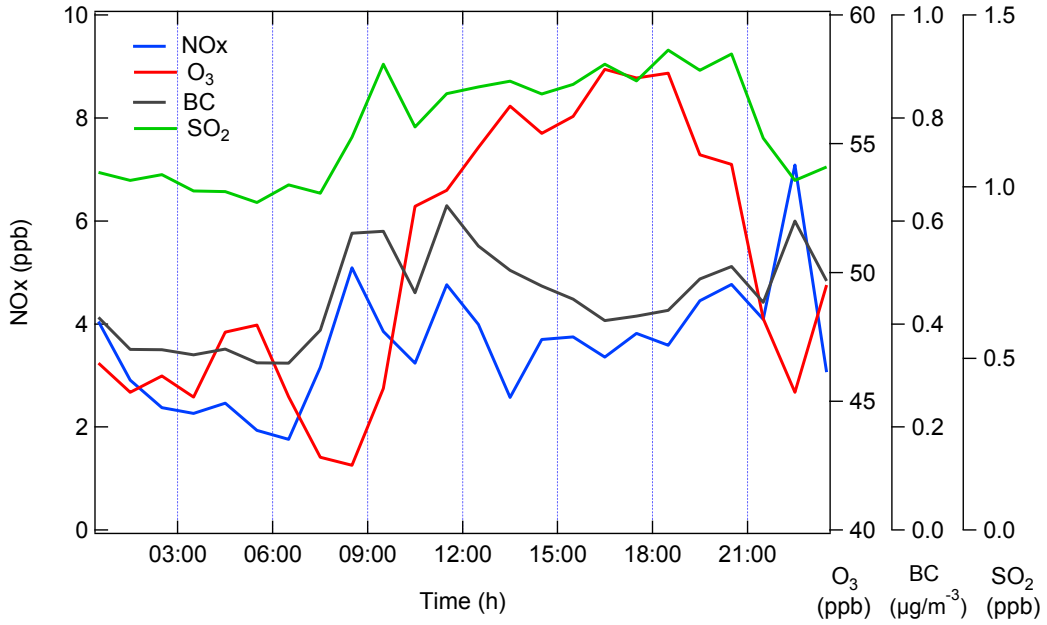

Figure S4. Diurnal profiles (median values of hourly averages) of nitrogen oxides (NO_x), black carbon (BC), sulfur dioxide (SO_2) and ozone (O_3) during the Patras summer campaign.

3. Athens summer campaign

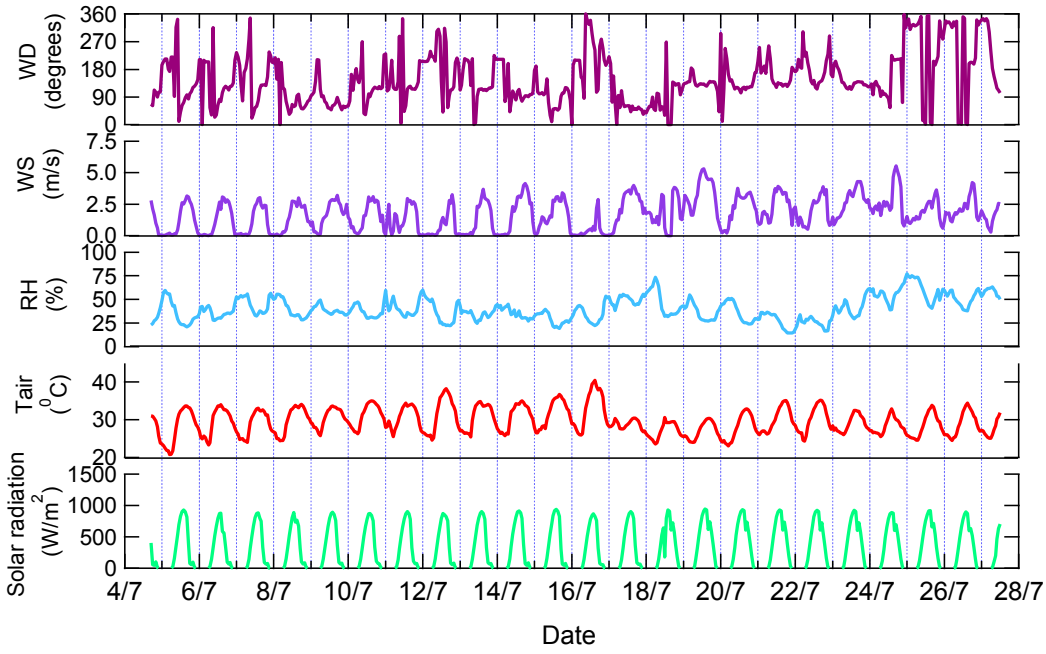

Figure S5. Meteorological conditions during the Athens summer campaign (hourly averages).

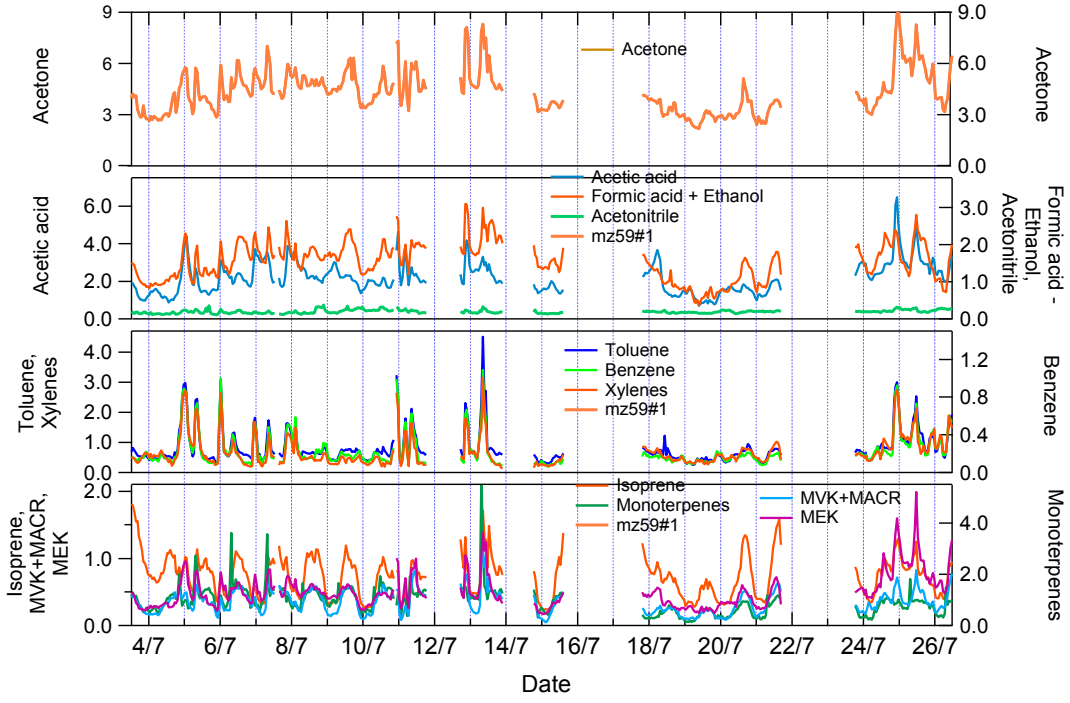

Figure S6. VOC time series for the Athens summer campaign (hourly averages). All values are in ppb.

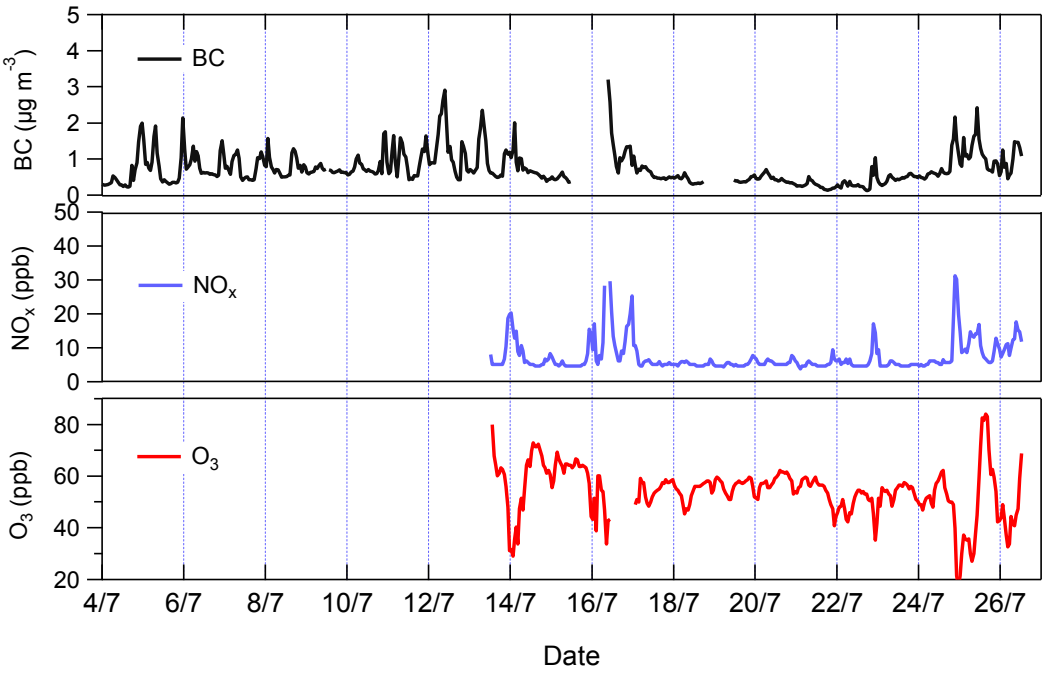

Figure S7. O_3 , NO_x and BC time series for the Athens summer campaign (hourly averages).

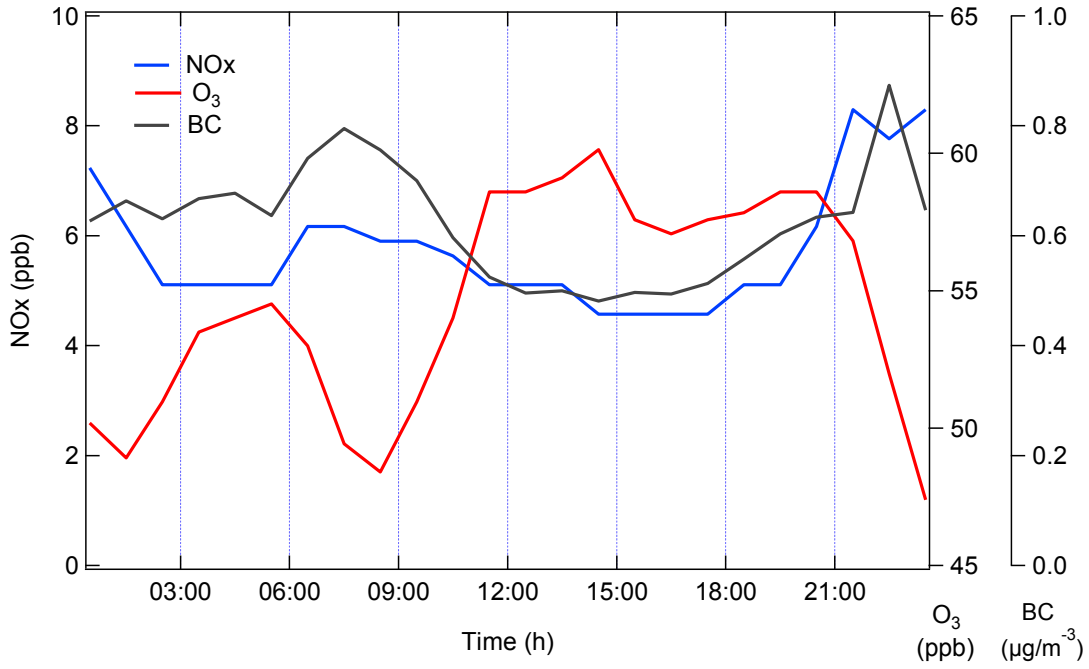

Figure S8. Diurnal profiles (median values of hourly averages) of nitrogen oxides (NO_x), black carbon (BC) and ozone (O_3) during the Athens summer campaign.

4. Athens winter campaign

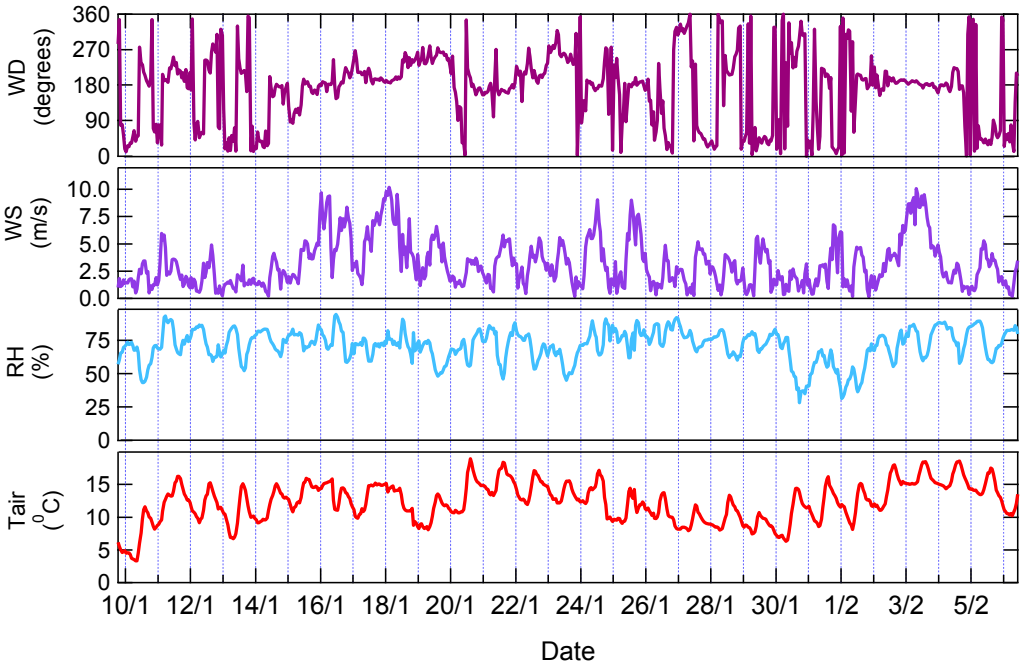

Figure S9. Meteorological conditions for the Athens winter campaign (hourly averages).

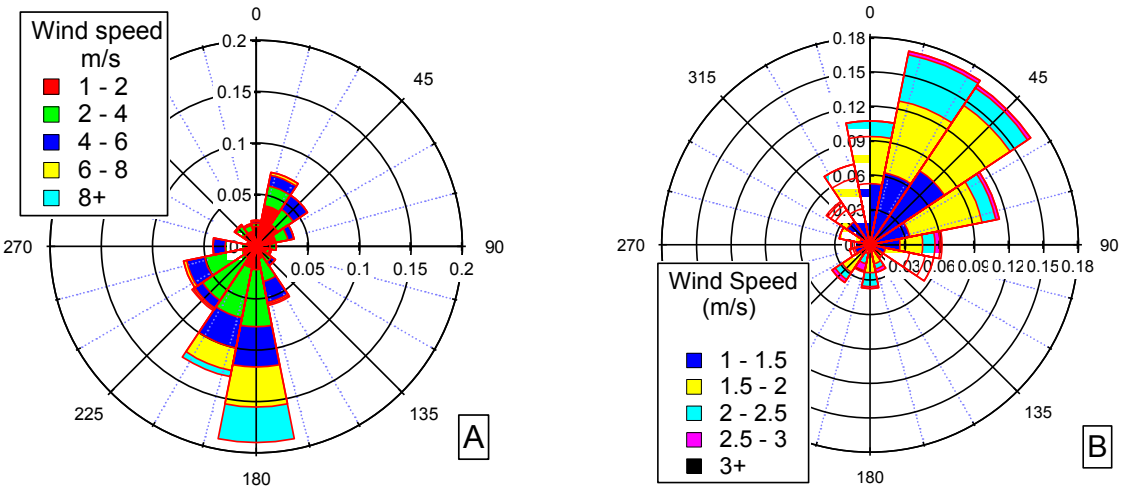

Figure S10. (A) Rose plots during the Athens winter campaign and (B) rose plots only during biomass burning periods (5 minute averages).

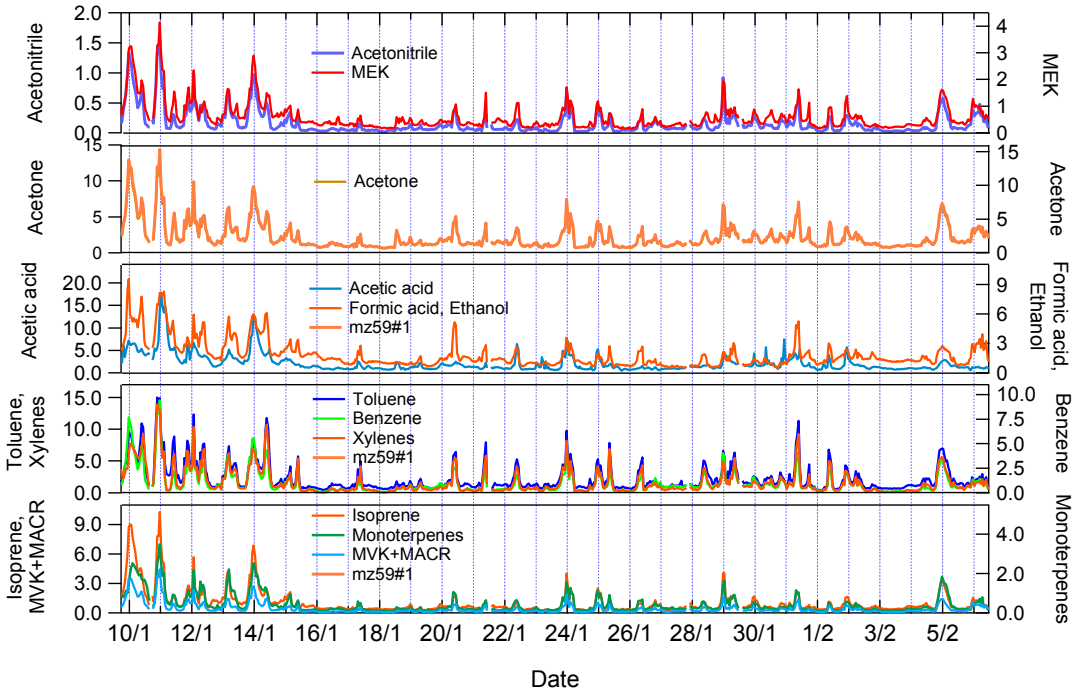

Figure S11. VOC time series for the Athens winter campaign (hourly averages). All values are in ppb.

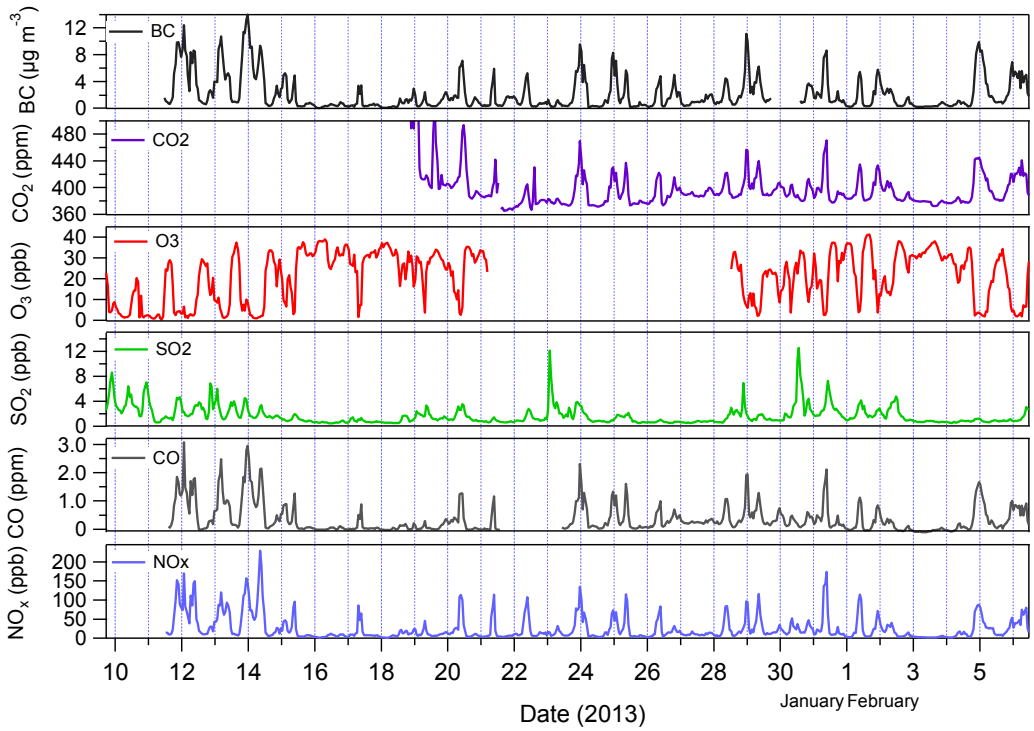

Figure S12. NO_x, CO, SO_2, O_3, CO_2 and BC time series for the Athens winter campaign (hourly averages).

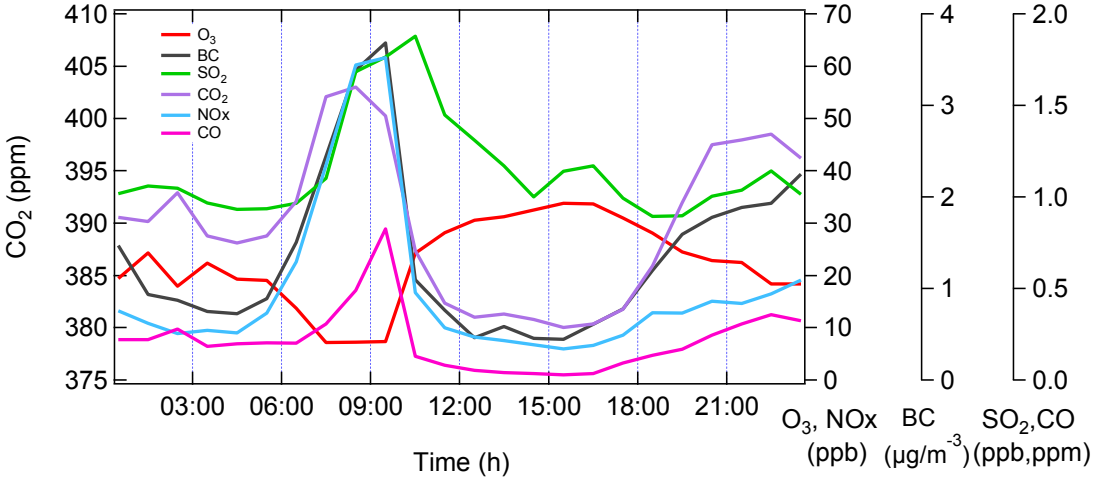

Figure S13. Diurnal profiles (median values) of nitrogen oxides (NO_x), black carbon (BC), ozone (O_3), sulfur dioxide (SO_2), carbon monoxide (CO) and carbon dioxide (CO_2) during the Athens winter campaign.

4.1 Periods of intense biomass burning

In order to select periods where biomass burning dominated the particulate and gas phase composition, daytime measurements were excluded, since contribution from traffic especially during morning rush hours is expected to influence the results. Measurements obtained only during nighttime (18:00-06:00 LT) were selected. For these nighttime measurements, background levels for acetonitrile were estimated based on the minimum acetonitrile, CO and CO_2 concentrations. For the above 'clean' periods the average value and standard deviation were estimated. The average acetonitrile value plus six times its standard deviation (=0.25 ppb) was used as a limit. Periods with acetonitrile levels above this limit were characterized as biomass burning periods. Biomass burning periods with duration more than 30 min were used for all the corresponding analyses in this work.

Table S2. Burning periods that met the criteria set for the Athens winter campaign.

Start	End	Duration (hh:mm)	Acetonitrile average (ppb)	Acetonitrile sd (ppb)
10/1/2013 19:00	11/1/2013 03:30	08:30	0.95	0.49
11/1/2013 18:25	12/1/2013 04:50	10:25	0.46	0.26
13/1/2013 02:25	13/1/2013 06:05	03:40	0.57	0.19
13/1/2013 18:55	14/1/2013 05:55	11:00	0.58	0.24
15/1/2013 01:50	15/1/2013 03:50	02:00	0.34	0.10
23/1/2013 20:45	24/1/2013 04:30	07:45	0.41	0.22
24/1/2013 22:10	25/1/2013 01:45	03:35	0.39	0.13
28/1/2013 22:45	29/1/2013 01:05	02:20	0.76	0.27
29/1/2013 22:30	29/1/2013 23:05	00:35	0.32	0.03
1/2/2013 21:40	1/2/2013 23:25	01:45	0.37	0.12
4/2/2013 20:05	5/2/2013 03:55	07:50	0.45	0.10
5/2/2013 22:20	6/2/2013 06:00	07:40	0.35	0.10

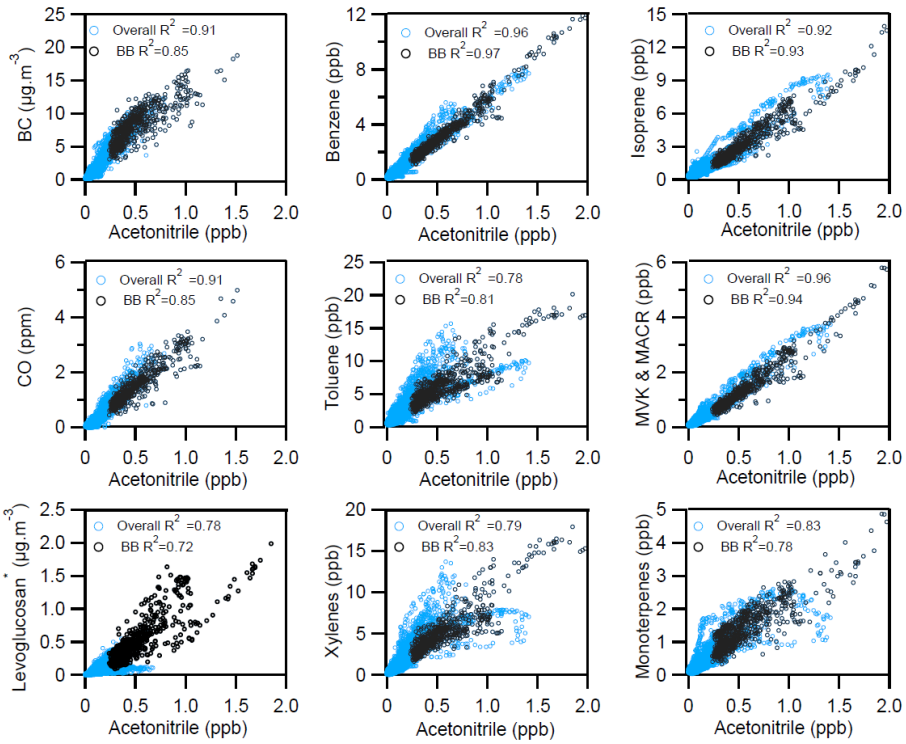

Figure S14. Scatter plots of acetonitrile versus particulate and gas species (BC, CO, levoglucosan (AMS m/z 60), benzene, toluene, xylenes, isoprene, MVK&MACR and monoterpenes) for the Athens winter campaign. Blue points indicate the overall measurement period. Black points indicate biomass burning periods. Overall R^2 values show the correlation of the species with acetonitrile for the overall measurement period. BB R^2 values show the correlation of the species with acetonitrile only for the biomass burning periods.

5. Patras summer campaign - PMF Analysis

5.1. Selection of the Number of factors

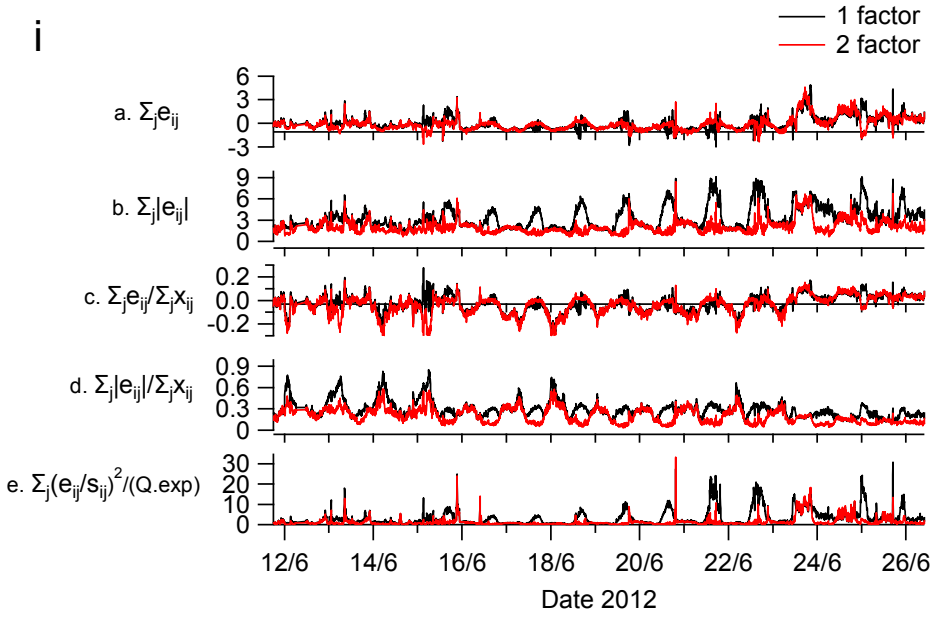

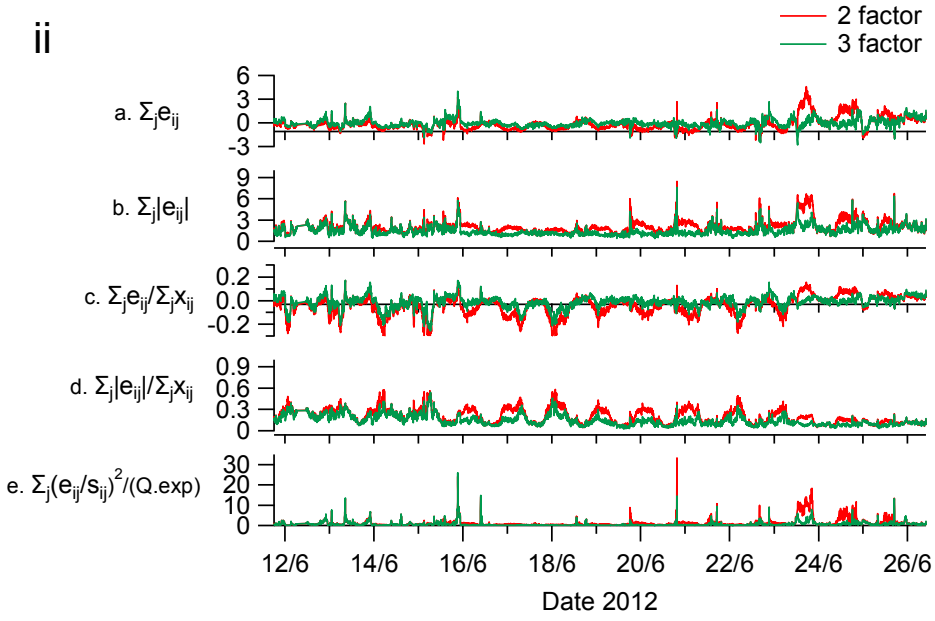

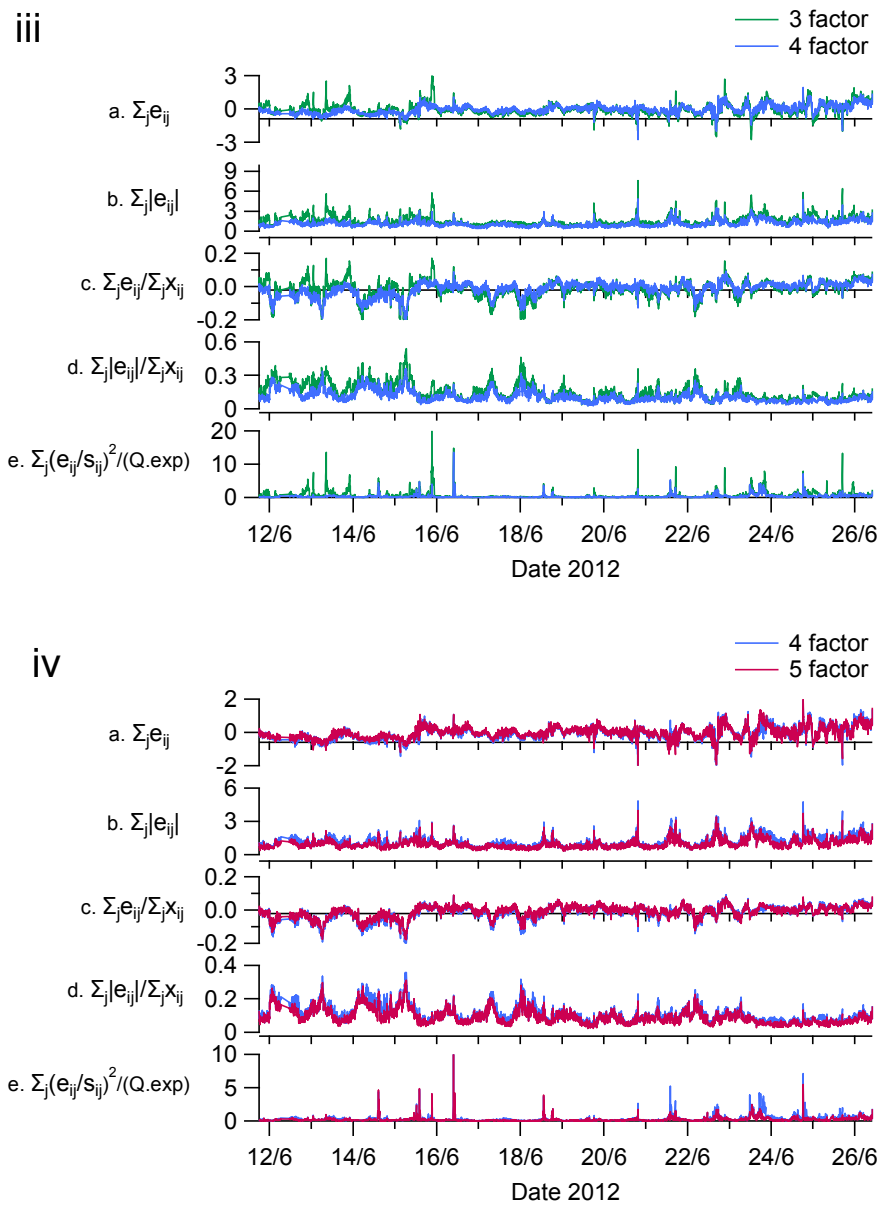

Figure S15. Selection of the number of factors for the Patras summer campaign. Comparison between model residuals **E= X-GF** (i) for 1-factor (black lines) and 2-factors (red lines) PMF solution, (ii) for 2-factors (red lines) and 3-factors (green lines) PMF solution, (iii) for 3-factor (green lines) and 4-factors (blue lines) PMF solution and (iv) for 4-factors (blue lines) and 5-factors (magenta lines) PMF solution. The model residuals were calculated as sums of (a) residuals, (b) the absolute value of residuals, (c) residuals relative to total VOCs, (d) absolute value of residuals relative to total VOCs, and (e) squared, uncertainty-weighted (scaled) residuals, Q(t)=E(t)/S(t), relative to expected values, Qexp(t). The model residuals were estimated using the PMF evaluation tool, PET, by Ulbrich et al. (2009). The structure in the residuals were decreased significantly in the p =2 solution compared to the p =1 solution. Comparing the 2 and 3 factor solutions the residuals had a significant decrease from the p=2 to the p=3 solution. A smaller decrease was observed for the p=3 to p=4 solution and a minimal decrease from the p=4 to p=5 solution. A 4 factor solution was selected.

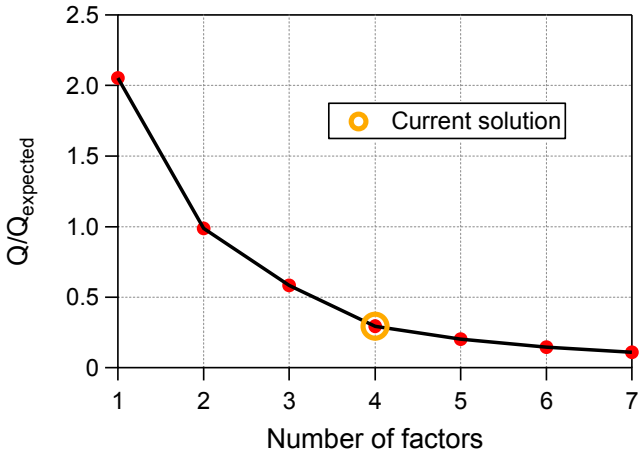

Figure S16. $Q/Q_{expected}$ versus the number of the factors for the Patras summer campaign.

5.2 Evaluation of solutions from the Patras summer campaign PMF in respect to the number of factors

5.2.1 3 factor solution - f_{peak} = 0.0

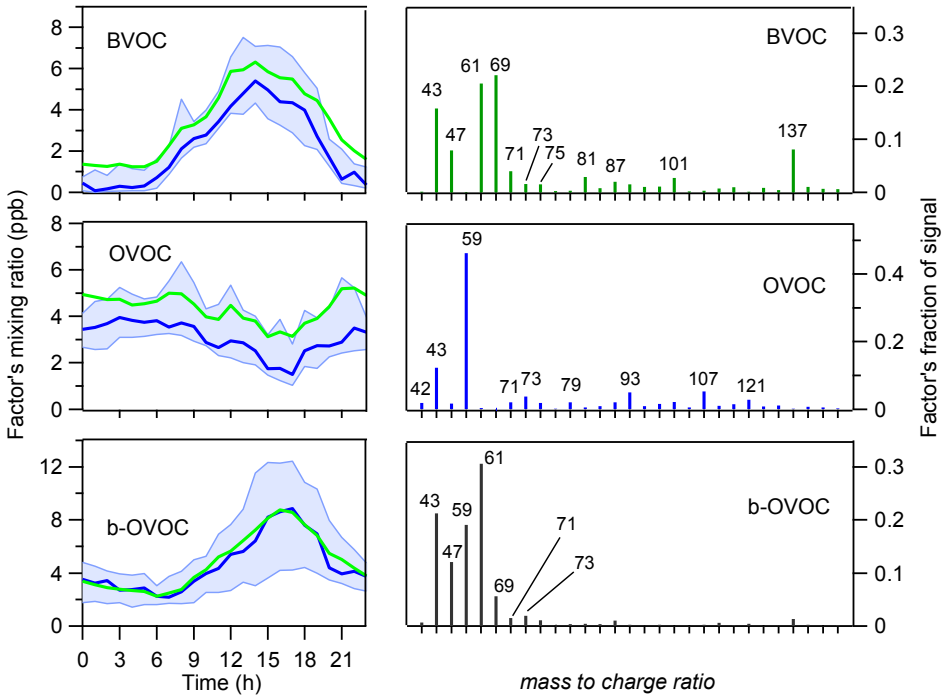

Figure S17. Diurnal profile and m/z distribution for the Patras summer campaign for the 3 factor solution.

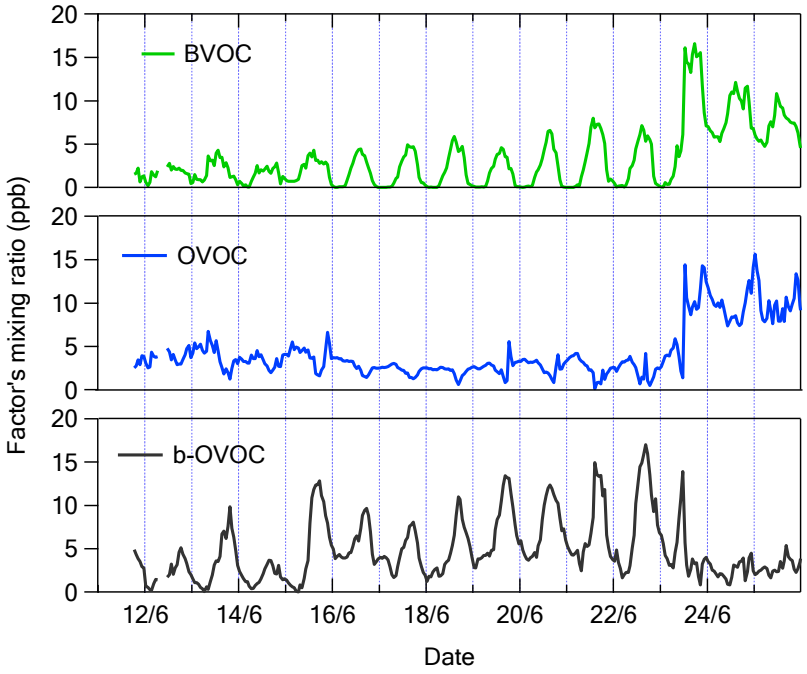

Figure S18. Time series of the 3 factors for the Patras summer campaign.

5.2.2 4 factor solution - f_{peak} = 0.0. (Proposed solution)

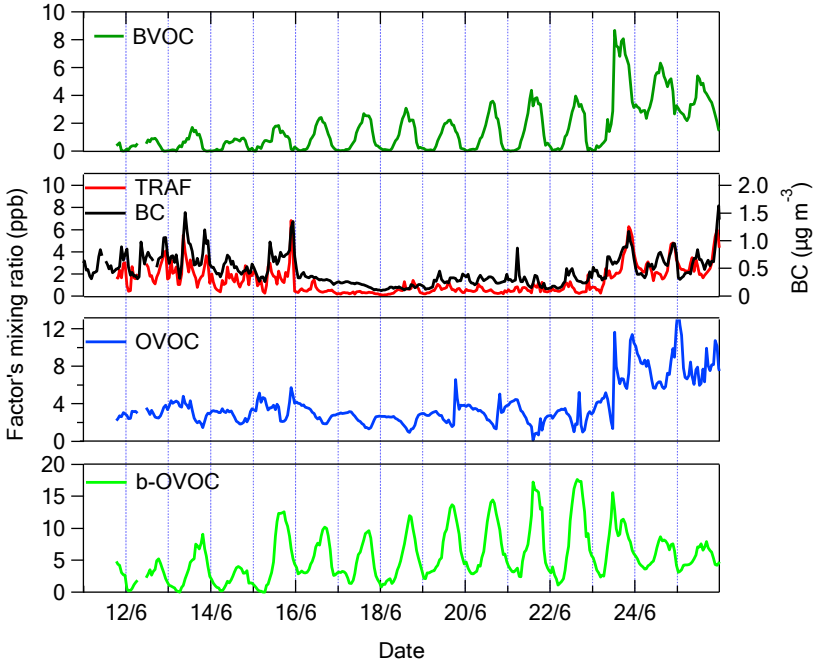

Figure S19. Patras summer campaign VOC factor time series. The BC concentration is also shown along with factor TRAF. The R^2 between TRAF to BC was 0.66.

5.2.3 5 factor solution - f_{peak} = 0.0

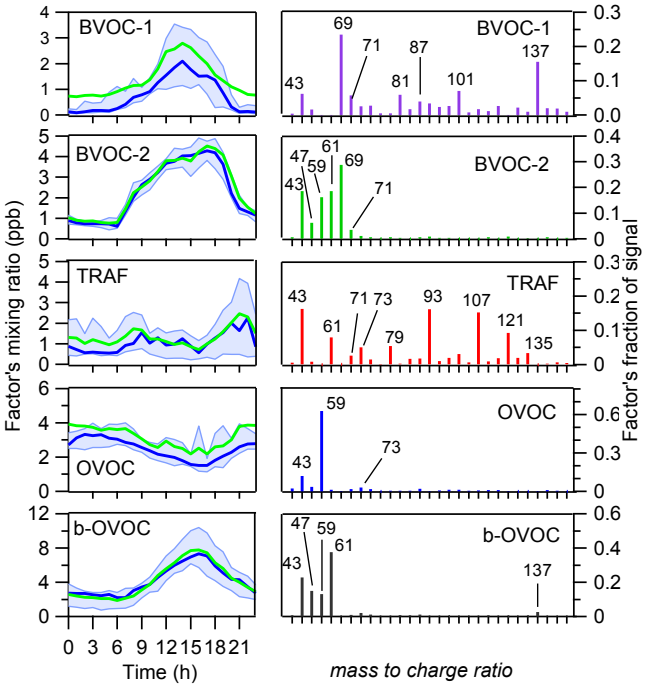

Figure S20. Diurnal profile and m/z distribution for the Patras summer campaign for the 5 factor solution.

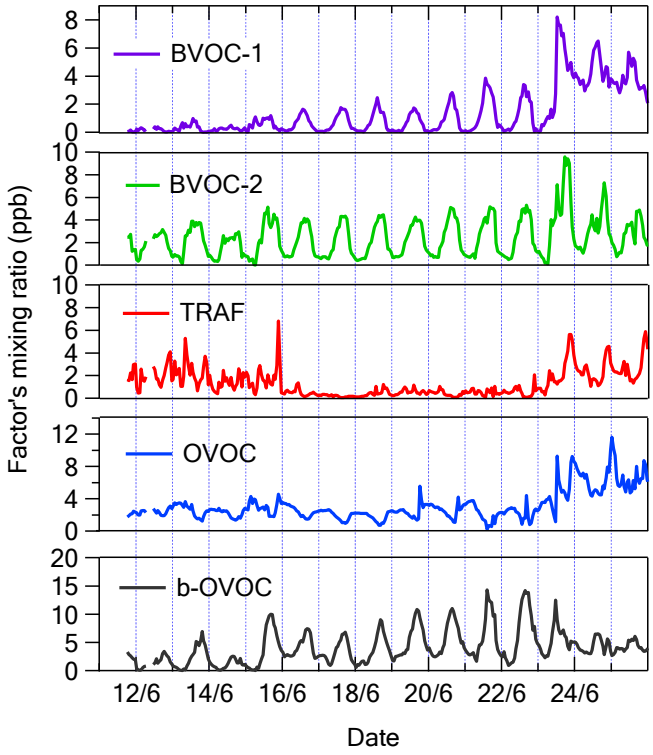

Figure S21. Time series of the 5 factors for the Patras summer campaign.

5.3 F_{peak} selection for the Patras summer campaign

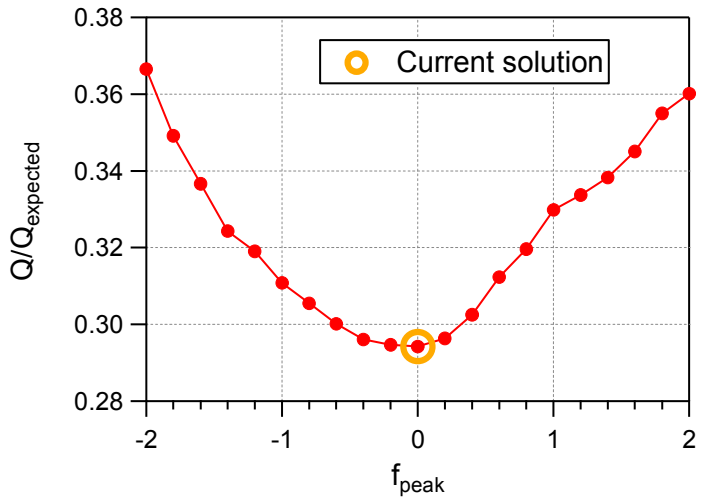

Figure S22. f_{peak} selection for Patras summer campaign. $Q/Q_{expected}$ for f_{peaks} -2 to 2 for a 4 factor solution. Values are stable between the f_{peak} -0.4 and 0.2.

i)

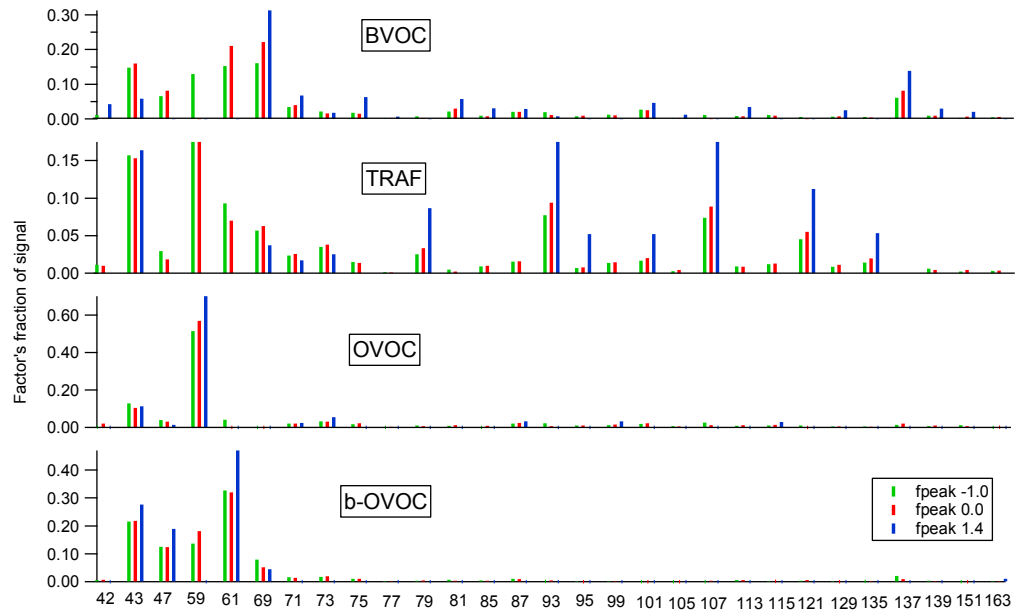

ii)

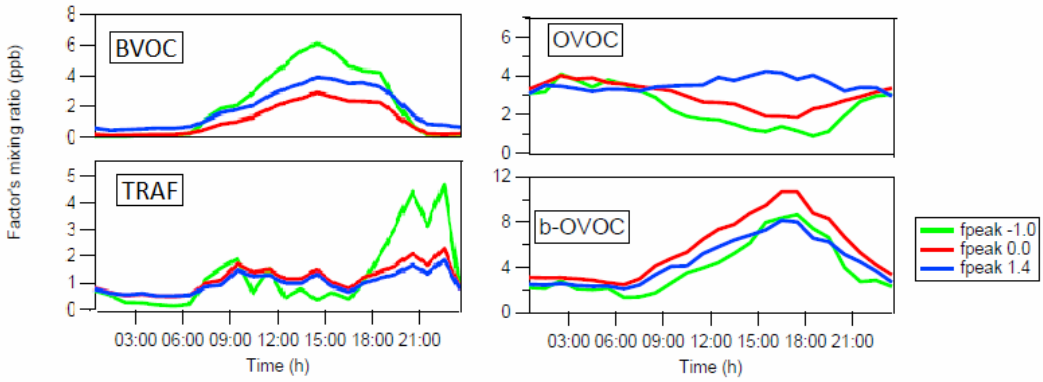

Figure S23. Other solutions for different fpeak values for the Patras summer campaign. **(i)** m/z contribution to the factors as a fraction of signal for each factor. Solutions for f_{peak} of -1.0, 0.2 and 1.4 are presented with green, red and blue color respectively. For the f_{peak} =1.4 solution all the acetone (*m/z* 59) is attributed to factor OVOC and all the acetic acid (*m/z* 61) is attributed to factor b-OVOC. **(ii)** Diurnal profiles (median values) of the factors for f_{peak} values of 0.2, -1.0 and 1.4. Diurnal profiles are similar to the presented factor solutions with the exception of the OVOC factor. This is mainly because of the contribution of acetone (*m/z* 59) that has been apportioned exclusively to this factor for an f_{peak} of 1.4 compared to the other solutions. The diurnal profile of the f_{peak} solution of 1.4 is similar to the acetone (*m/z* 59) diurnal profile.

5.4 Wind direction dependence of the PMF factors

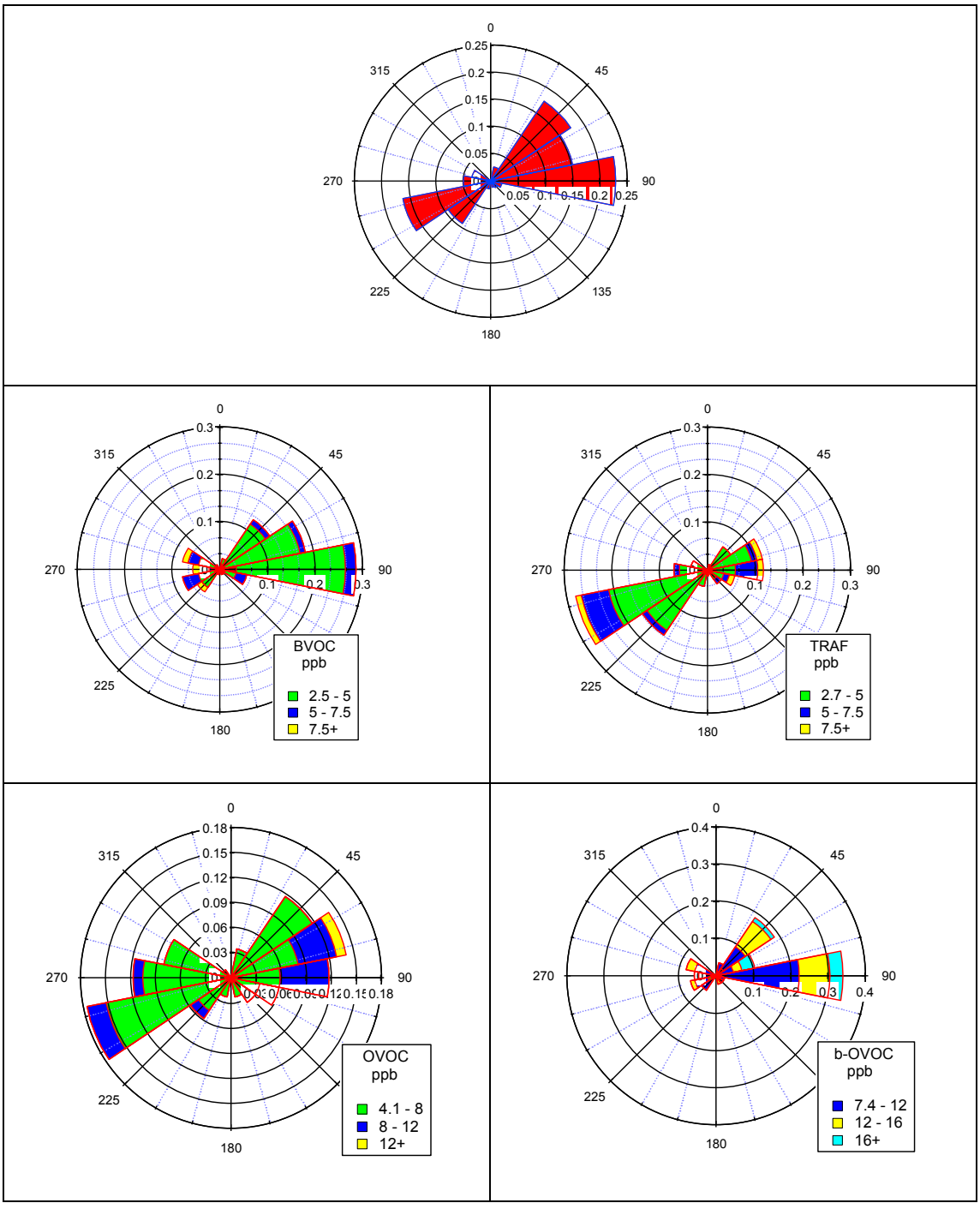

Figure S24 Rose plots for wind direction, and the PMF factors for values above the 75% percentile.

6. Athens summer campaign - PMF Analysis

6.1. Selection of the number of factors

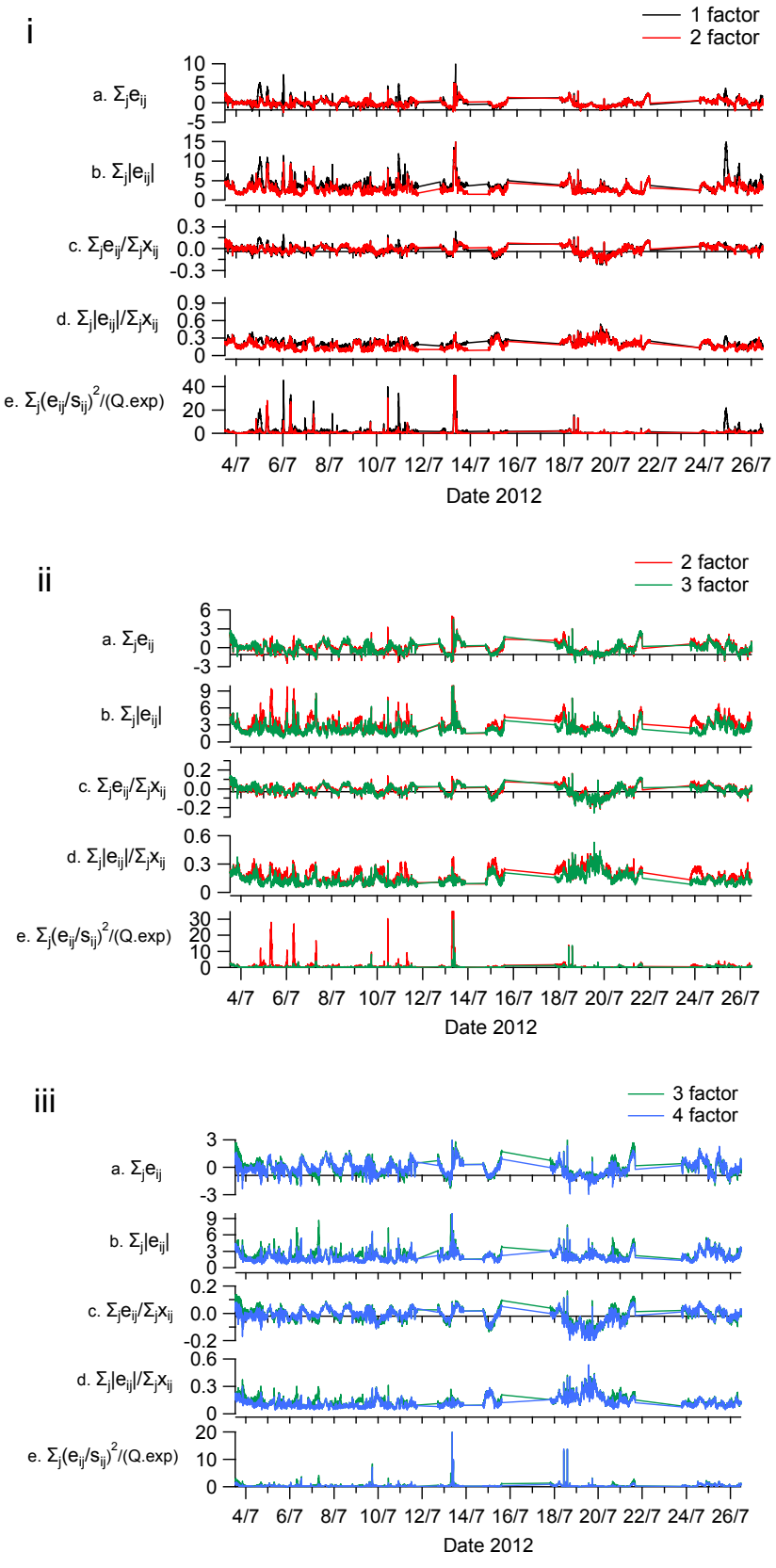

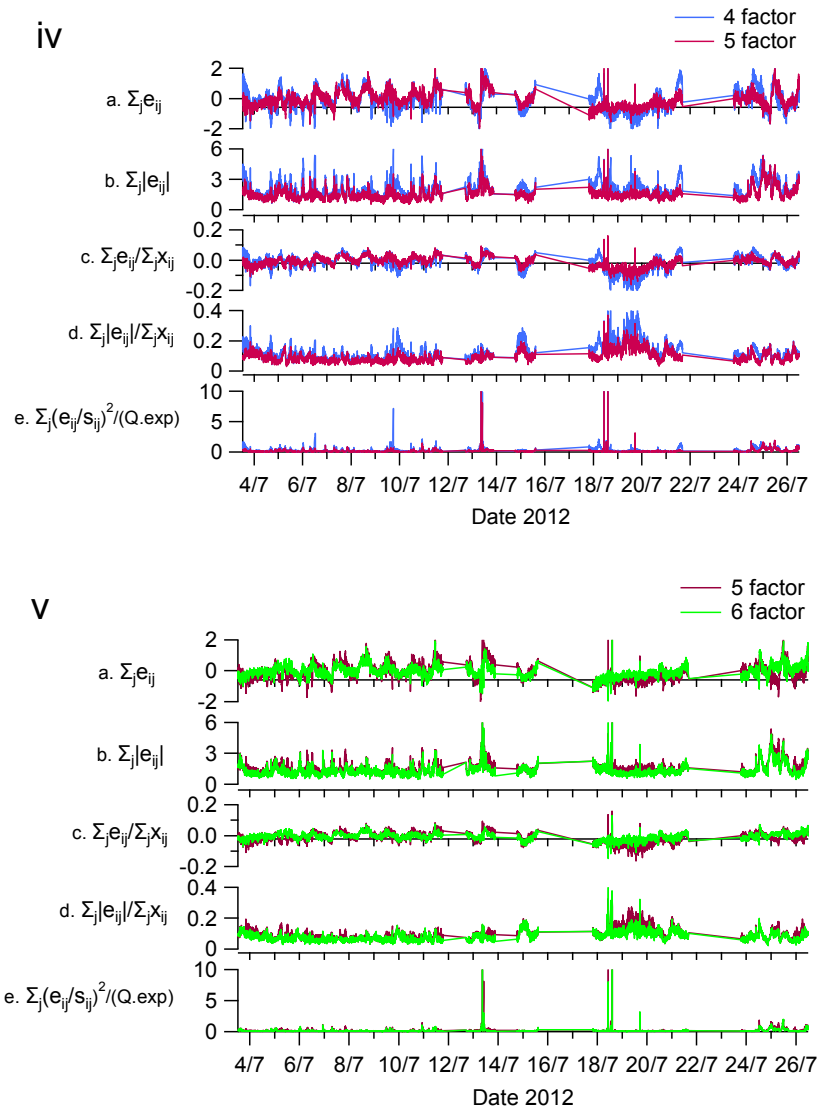

Figure S25. Selection of the number of factors for the Athens summer campaign. Comparison between model residuals **E= X-GF** (i) for 1-factor (black lines) and 2-factors (red lines) PMF solution, (ii) for 2-factors (red lines) and 3-factors (green lines) PMF solution, (iii) for 3-factor (green lines) and 4-factors (blue lines) PMF solution, (iv) for 4-factors (blue lines) and 5-factors (magenta lines) PMF solution and (v) for 5-factors (magenta lines) and 6-factors (light green lines) PMF solution. The model residuals were calculated as sums of: (a) residuals, (b) the absolute value of residuals, (c) residuals relative to total VOCs, (d) absolute value of residuals relative to total VOCs, and (e) sum of squared, uncertainty-weighted (scaled) residuals, Q(t)=E(t)/S(t), relative to expected values, Qexp(t). A 5 factor solution was selected.

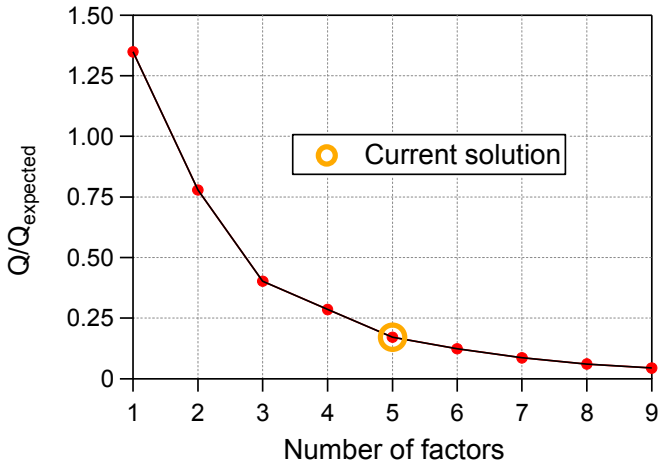

Figure S26. $Q/Q_{expected}$ versus the number of the factors for the Athens summer campaign.

6.2 Evaluation of solutions from the Athens summer campaign PMF in respect to the number of factors.

6.2.1 4 factor solution - f_{peak} = 0.0.

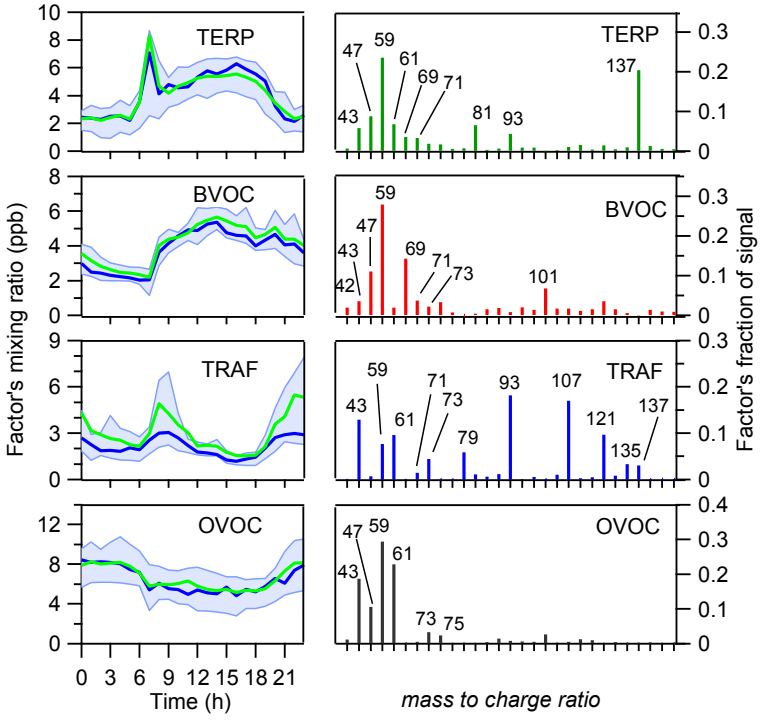

Figure S27. Diurnal profile and m/z distribution for the Athens summer campaign for the 4 factor solution.

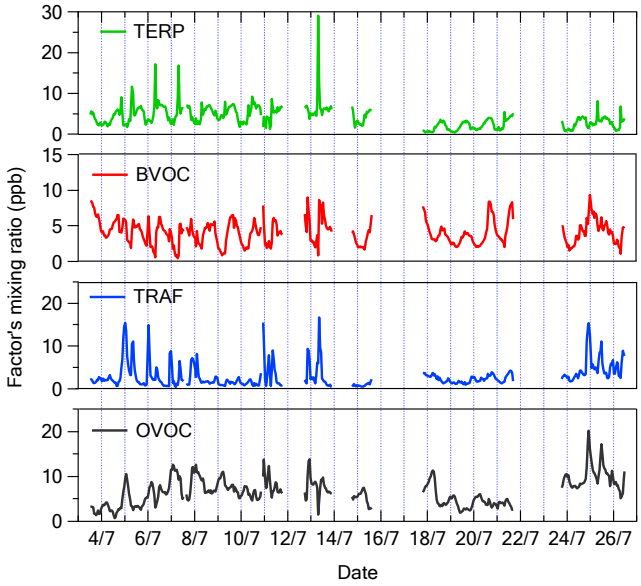

Figure S28. Time series of the 4 factors for the Athens summer campaign.

6.2.2. 5 factor solution - f_{peak} = 0.0 for Athens summer campaign.

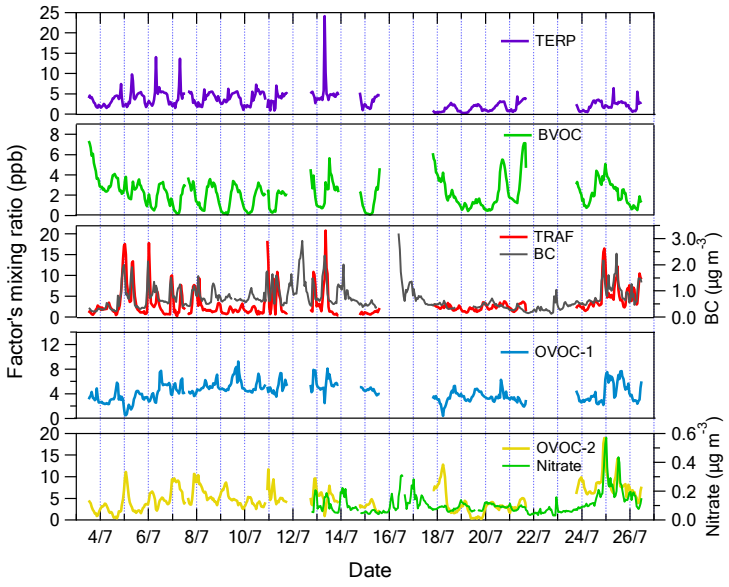

Figure S29. Athens summer campaign PMF. Factors' time-series and correlations with other species. Correlation between factor TRAF and BC was 0.45 (R^2). Factor OVOC-2 correlates with AMS's NO_3 (R^2=0.43).

6.2.3. 6 factor solution - f_{peak} = 0.0 for Athens summer campaign

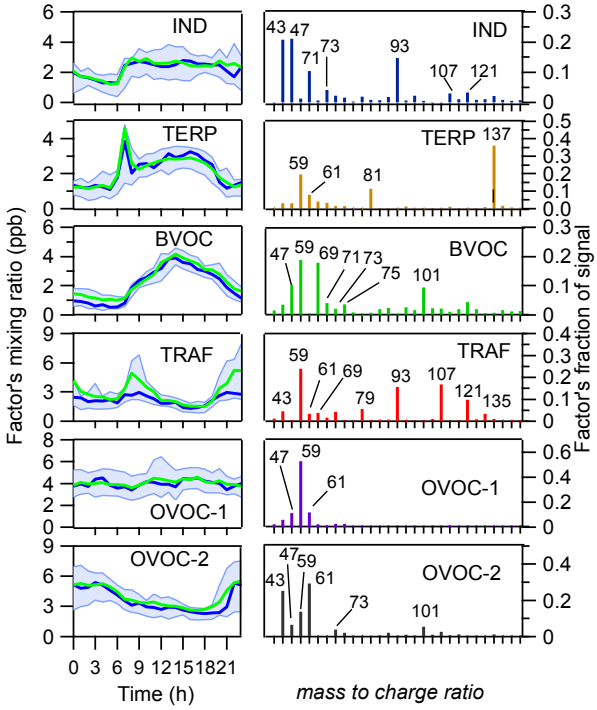

Figure S30. Diurnal profile and m/z distribution for the Athens summer campaign for the 6 factor solution.

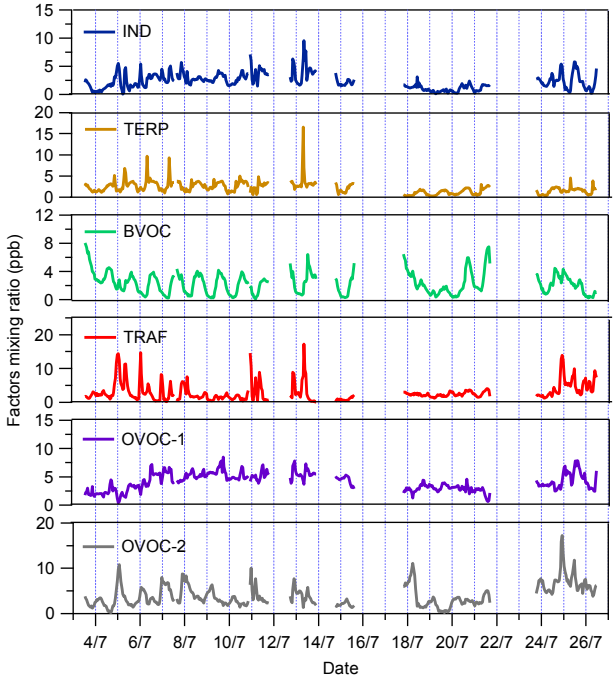

Figure S31. Time series of the 6 factors for the Athens summer campaign.

The factors proposed by this solution include an additional one (factor IND) that mainly contains toluene and some smaller VOCs. This factor is elevated during the day and could be related to industrial processes and/or traffic.

6.3 F_{peak} selection for the Athens summer campaign

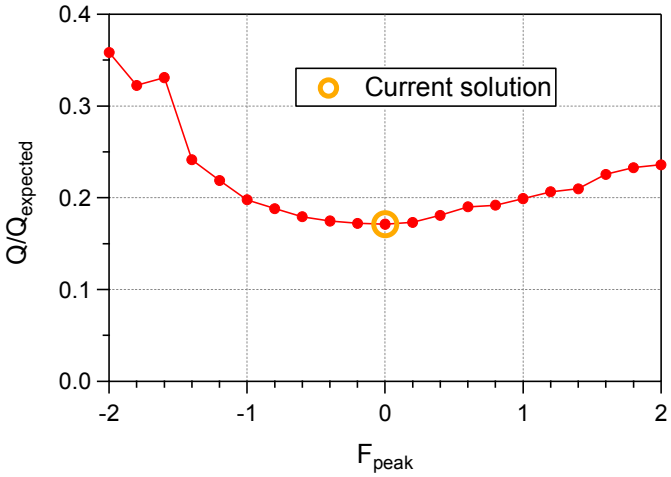

Figure S32. f_{peak} selection for the Athens summer campaign. $Q/Q_{expected}$ for f_{peak} -2 to 2 for the 5 factor solution. Values are stable between f_{peak} -0.6 and 0.4.

i)

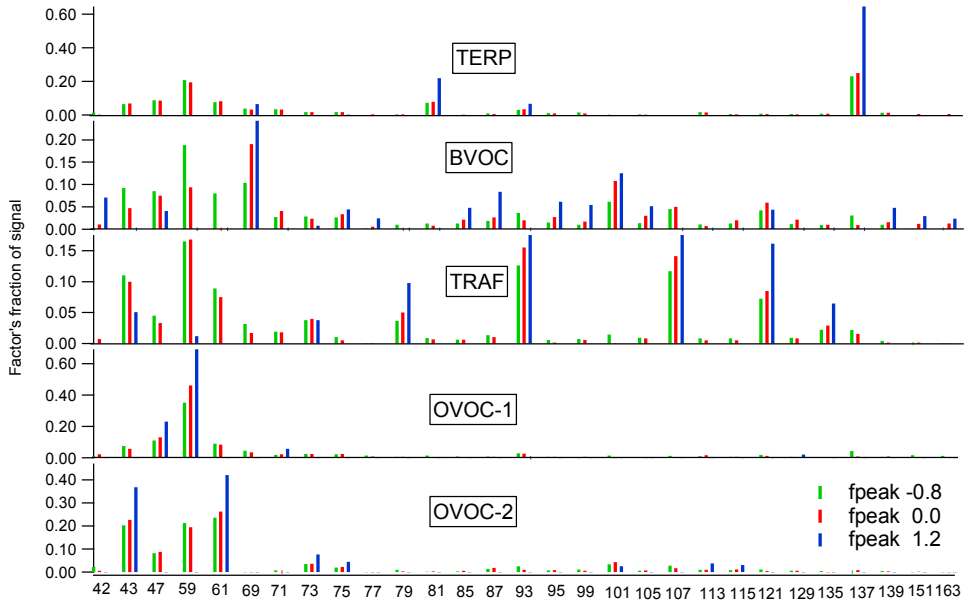

ii)

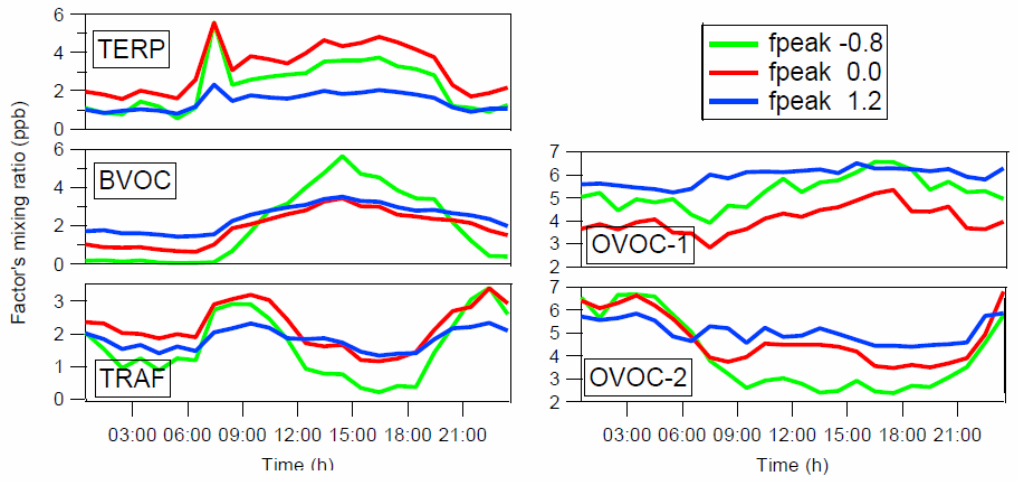

Figure S33. Solutions for other f_{peak} values for the Athens summer campaign**. (i)** M/z contribution to the factors as a fraction of signal for each factor. Solutions for fpeak of -0.8, 0.0 and 1.2 are presented with green, red and blue color respectively. **(ii)** Diurnal profiles of the factors for f_{peak} solutions of -0.8, 0.0 and 1.2. Diurnal profiles follow the same trend in all cases.

6.4 **Wind direction dependence of the PMF factors**

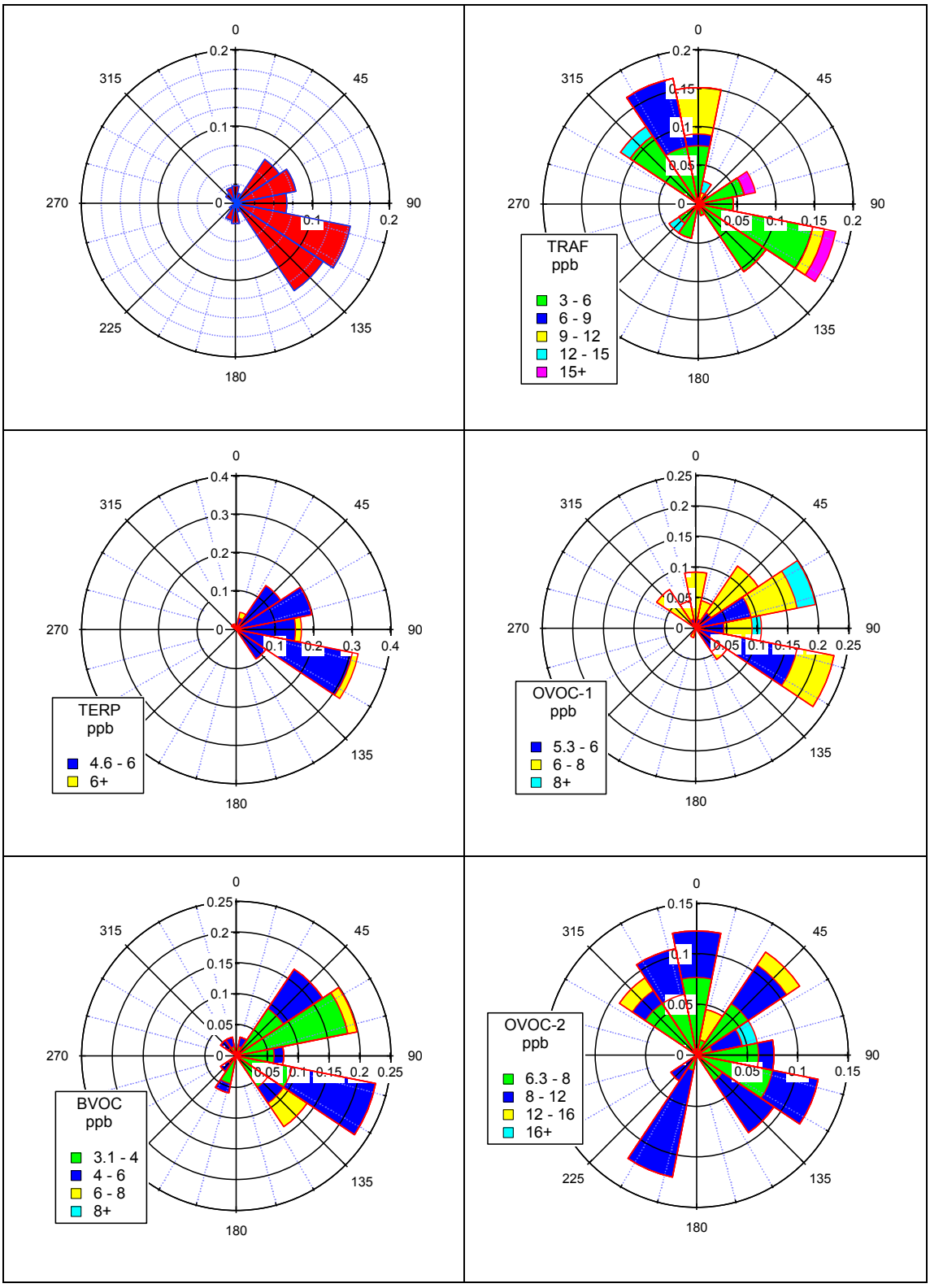

Figure S34. Rose plots for wind direction, and the PMF factors for values above the 75% percentile.

7. Athens winter campaign - PMF Analysis

7.1 Selection of the Number of factors for the Athens winter campaign

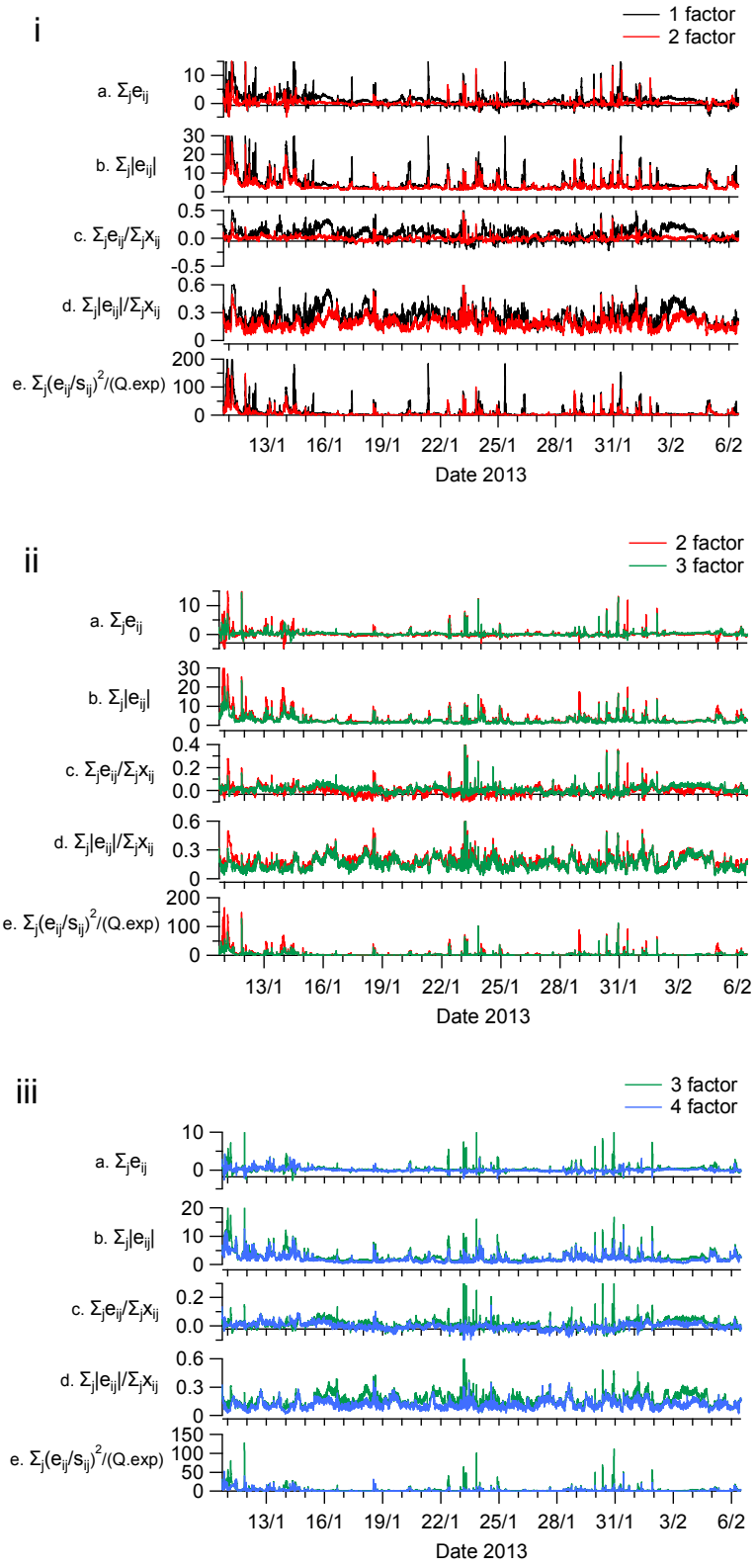

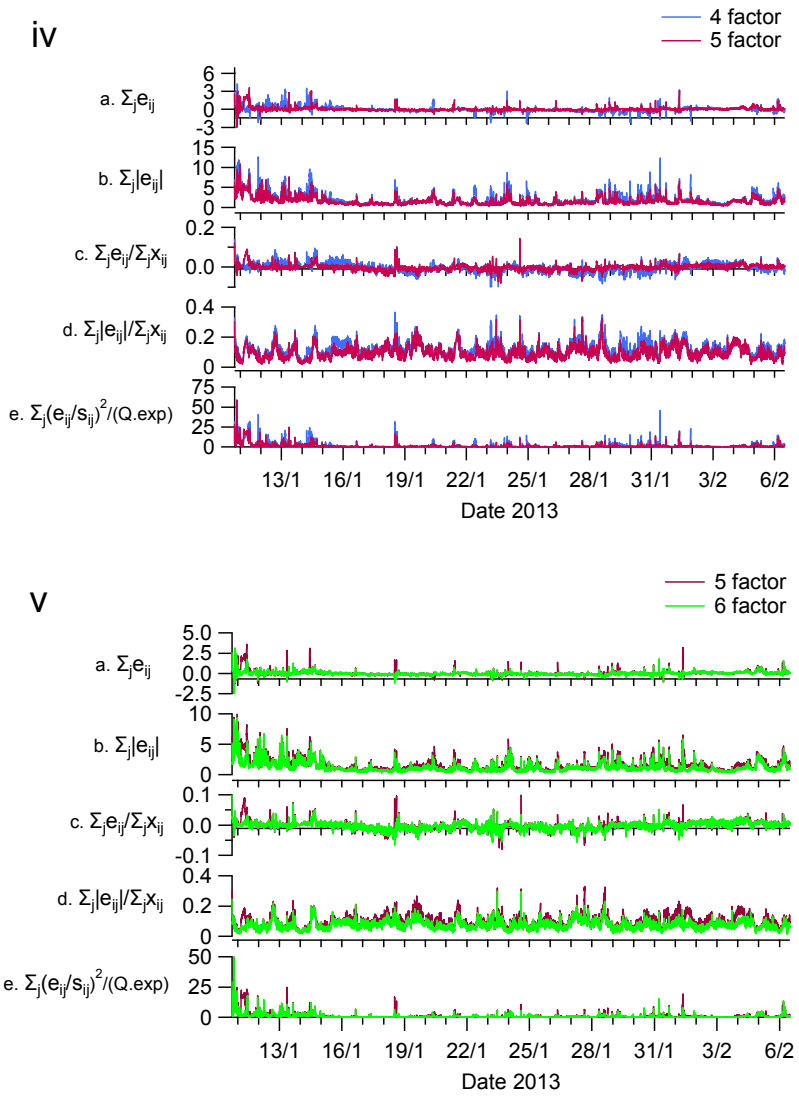

Figure S35. Selection of the number of factors for the Athens summer campaign. Comparison between model residuals **E= X-GF** (i) for 1-factor (black lines) and 2-factors (red lines) PMF solution, (ii) for 2-factors (red lines) and 3-factors (green lines) PMF solution, (iii) for 3-factor (green lines) and 4-factors (blue lines) PMF solution, (iv) for 4-factors (blue lines) and 5-factors (magenta lines) PMF solution, and (v) for 5-factors (magenta lines) and 6-factors (light green lines) PMF solution. The model residuals were calculated as sums of: (a) residuals, (b) the absolute value of residuals, (c) residuals relative to total VOCs, (d) absolute value of residuals relative to total VOCs, and (e) squared, uncertainty-weighted (scaled) residuals, Q(t)=E(t)/S(t), relative to expected values, Qexp(t). A 5 factor solution was selected.

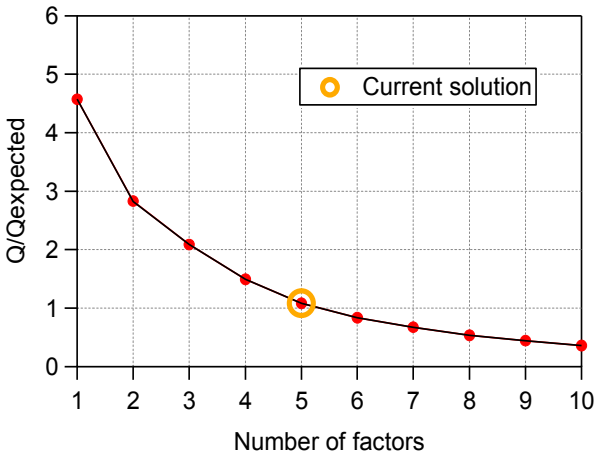

Figure S36. $Q/Q_{expected}$ versus the number of the factors for the Athens winter campaign.

7.2 Evaluation of solutions from the Athens winter campaign PMF

7.2.1 4 factor solution - f_{peak} = 0.0 for Athens winter campaign

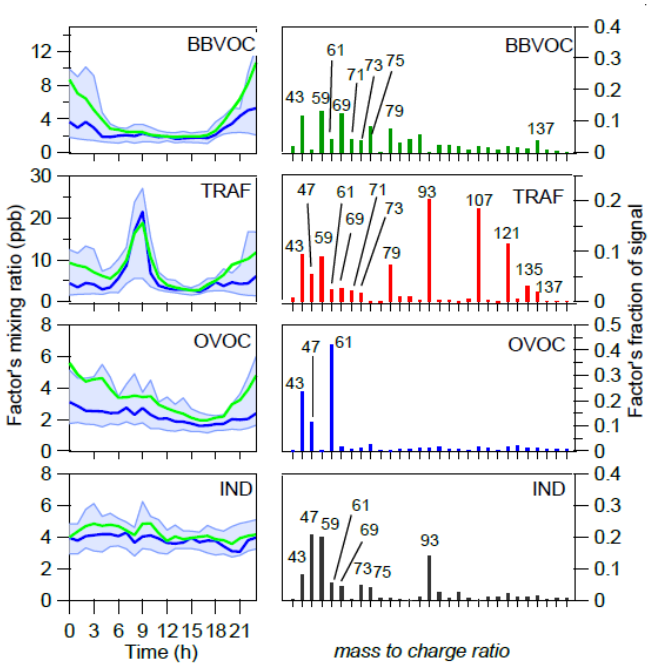

Figure S37. Diurnal profile and m/z distribution for the Athens winter campaign for the 4 factor solution.

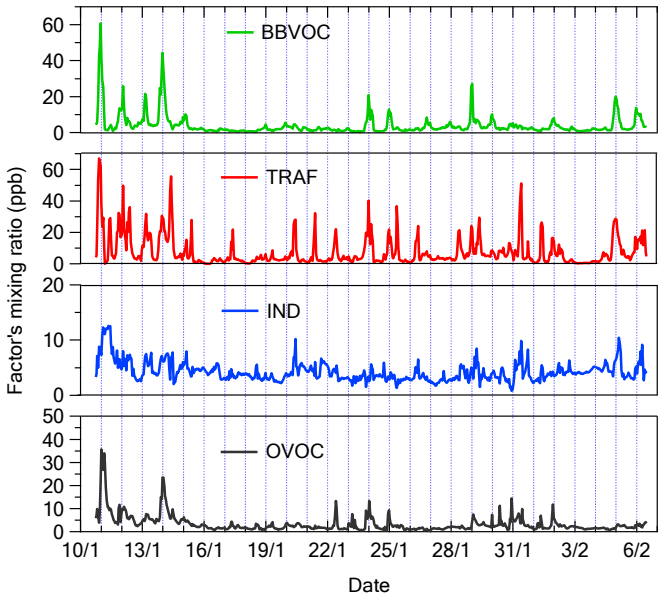

Figure S38. Time series of the 4 factors for the Athens winter campaign.

7.2.2. 5 factor solution - f_{peak} = 0.0 for the Athens winter campaign (selected solution)

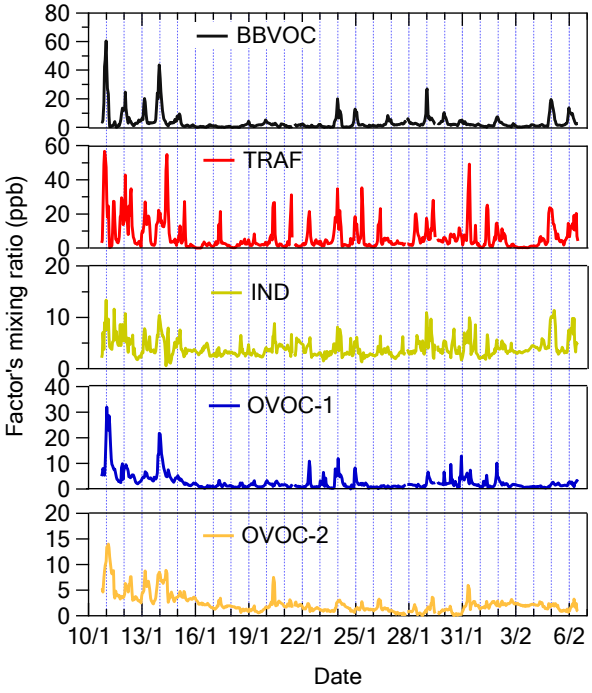

Figure S39. Time series of the 5 factors for the Athens winter campaign.

7.2.3. 6 factor solution – f_{peak} = 0.0 for Athens winter campaign

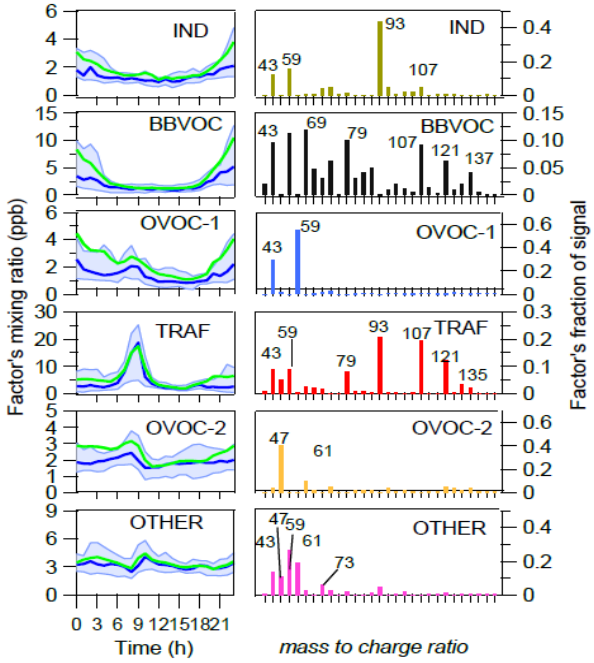

Figure S40. Diurnal profile and m/z distribution for the Athens winter campaign for the 6 factor solution.

7.3. PMF analysis for the Athens winter campaign including the first day.

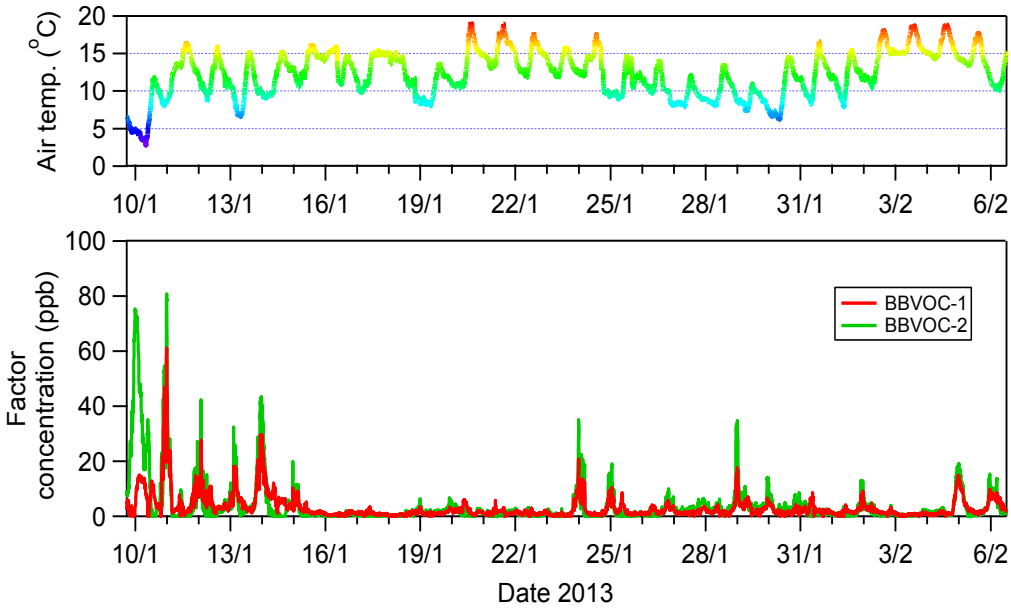

Figure S41. Timeseries of temperature, BBVOC-1, and BBVOC-2 for the 6 factor solution of the Athens winter campaign (including fist day).

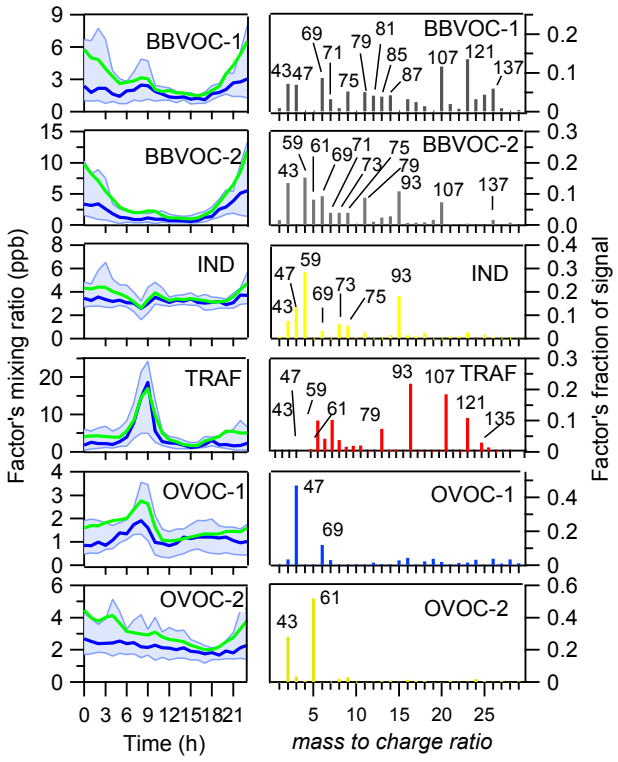

Figure S42. Diurnal profile and m/z distribution for the Athens winter campaign (including first day) for the 6 factor solution.

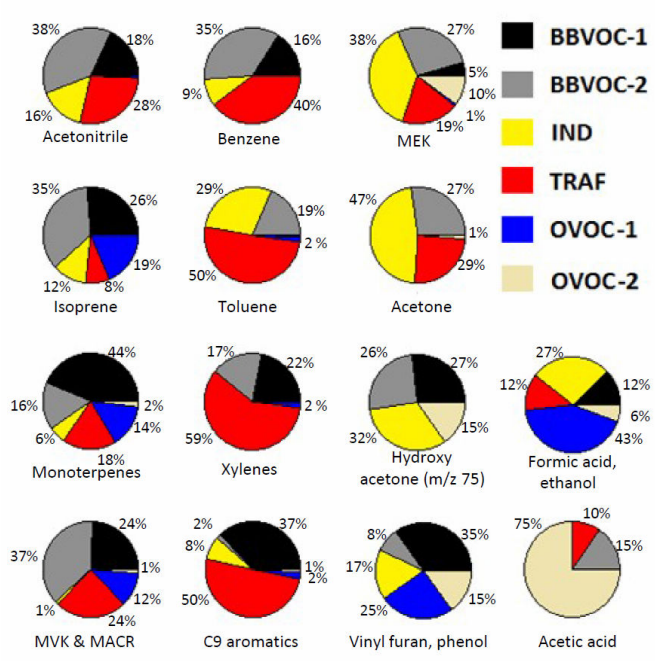

Figure S43. Species percentage (%) attributed to the PMF factors for Athens winter campaign (including first day) for the 6 factor solution.

7.4 F_{peak} selection for Athens winter campaign.

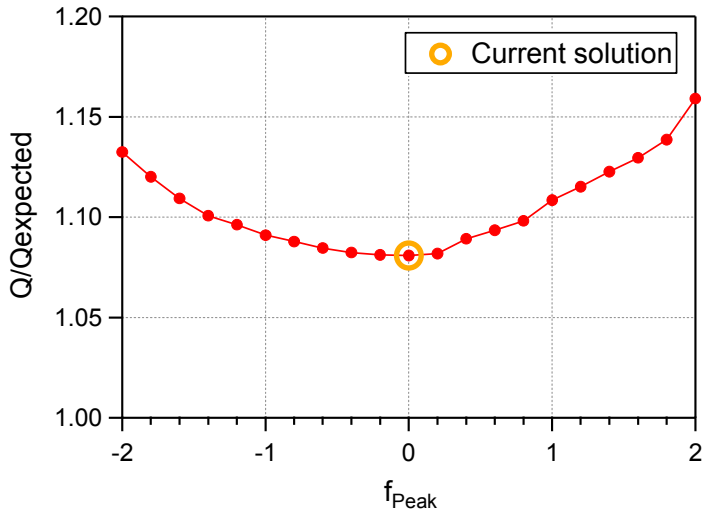

Figure S44. f_{peak} selection. $Q/Q_{expected}$ for f_{peak} -2 to 2 for the factor solution for Athens winter campaign. Values are stable between the f_{peak} -0.4 and 0.2.

i)

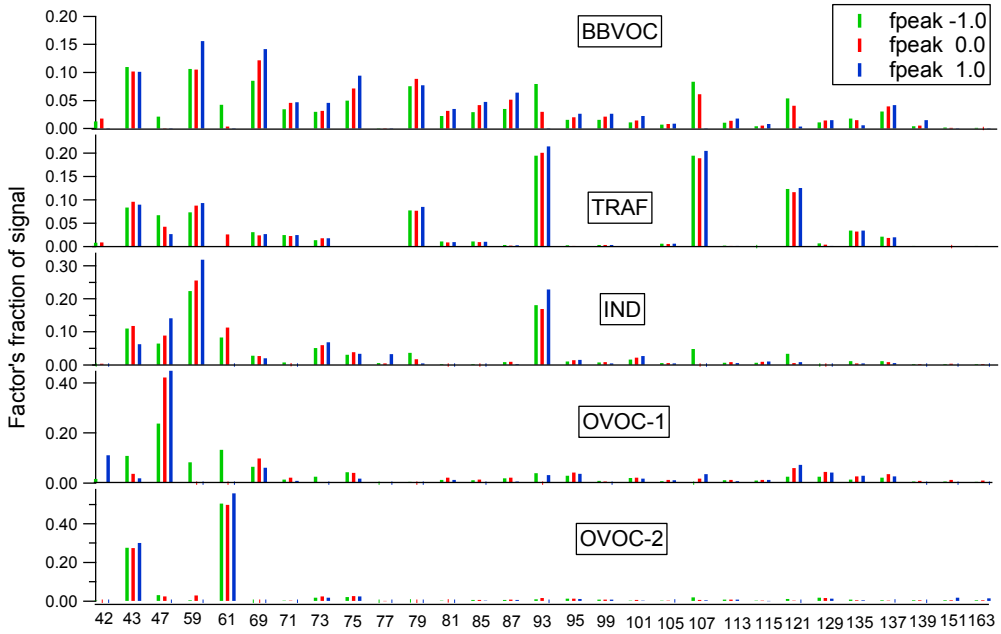

ii)

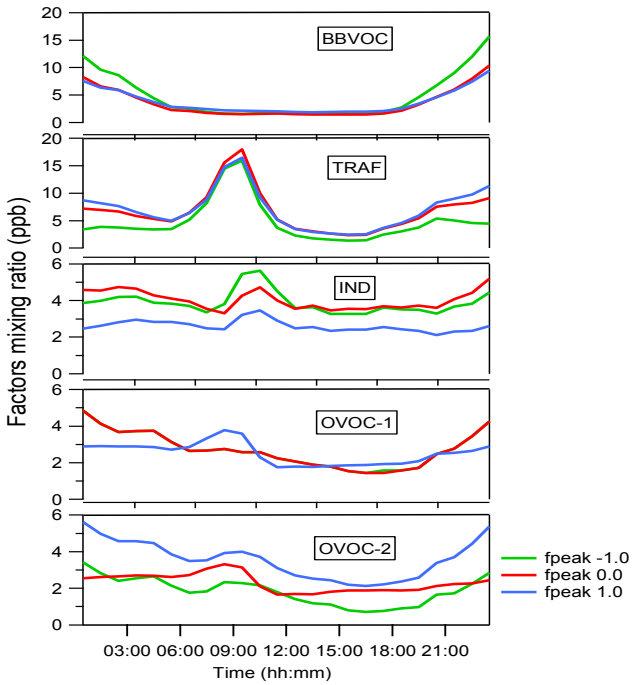

Figure S45. Other f_{peak} solutions for the Athens winter campaign. **(i)** M/z contribution to the factors as a fraction of signal for each factor. Solutions for f_{peak} of -1.0, 0.0 and 1.0 are presented with green, red and blue color respectively. **(ii)** Diurnal profiles of the factors for the above f_{peak} solutions.

7.5 Wind direction dependence of the PMF factors

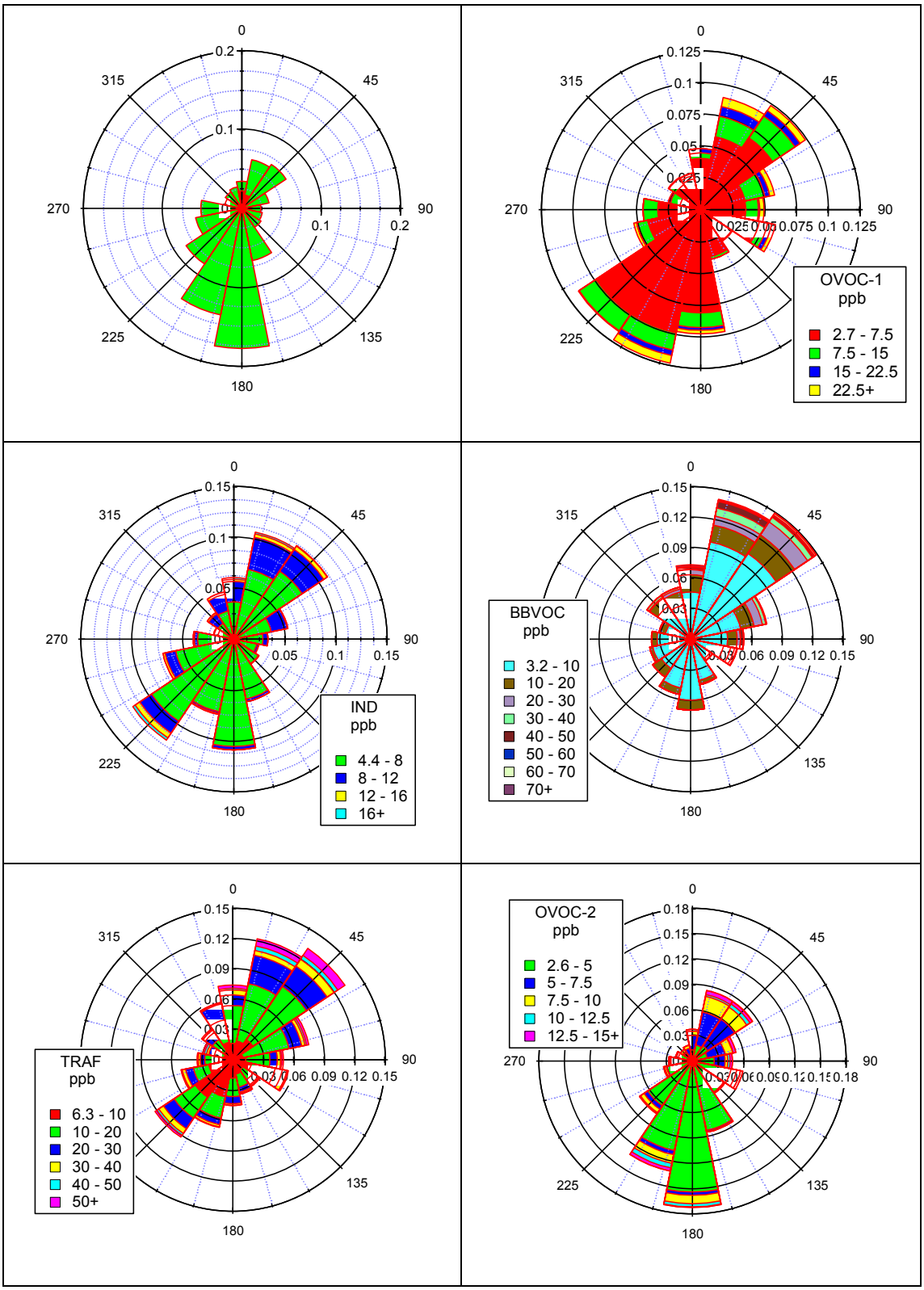

Figure S46. Rose plots for wind direction, and the PMF factors for values above the 75% percentile

8. PMF overview

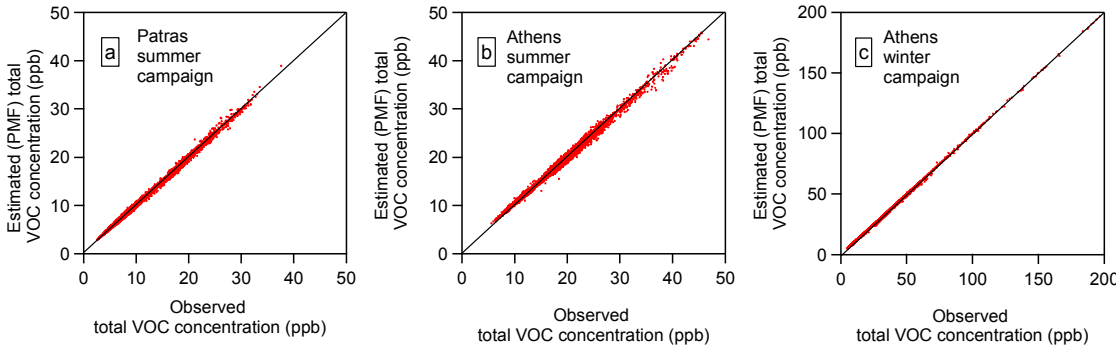

Figure S47. Predicted (PMF) vs observed total VOC concentrations for the three campaigns.

References

Christian, T.J., Kleiss, B., Yokelson, R.J. and Holzinger, R.: Comprehensive laboratory measurements of biomass-burning emissions: 2. First intercomparison of open-path FTIR, PTR-MS, and GC-MS/FID/ECD. Journal of Geophysical Research, 109, D02311, doi: 10.1029/2003JD003874, 2004.

DeGouw, J. A., Goldan, P. D., Warneke, C., Kuster, W. C., Roberts, J. M., Marchewka, M., Bertman, S. B., Pszenny, A. A. P., and Keene, W. C.: Validation of proton transfer reaction-mass spectrometry (PTR-MS) measurements of gas-phase organic compounds in the atmosphere during the New England Air Quality Study (NEAQS) in 2002. Journal of Geophysical Research, 108, 4682, doi: 10.1029/2003JD003863, 2003.

DeGouw, J. and Warneke, C.: Measurements of volatile organic compounds in the earth's atmosphere using proton-transfer-reaction mass spectrometry. Mass Spectrometry Reviews, 26, 223– 257, 2007.

Holzinger, A., Lee, A., Paw, K.T., and Goldstein, A.H.: Observations of oxidation products above a forest imply biogenic emissions of very reactive compounds. Atmos. Chem. Phys., 5, 67–75, 2005a.

Holzinger, R., Williams, J., Salisbury, G. Klupfel, deReus, T., Traub, M., Crutzen, P. and Lelieveld, J.: Oxygenated compounds in aged biomass burning plumes over the Eastern Mediterranean: evidence for strong secondary production of methanol and acetone. Atmos. Chem. Phys., 5, 39–46, 2005b.

Karl, T., Crutzen, P.J., Mandl, M., Staudinger, M., Guenther, A., Jordan,A., Fall, R. and Lindinger, W.: Variability-lifetime relationship of VOCs observed at the Sonnblick Observatory 1999 - estimation of HO-densities. Atmospheric Environment 35, 5287–5300, 2001.

Karl, T., Jobson, T., Kuster, W.C.,Williams, E., Stutz, J., Shetter, R., Hall, S.R., Goldan, P., Fehsenfeld, F. and Lindinger, W.: Use of proton-transfer-reaction mass spectrometry to characterize volatile organic compound sources at the La Porte super site during the Texas Air Quality Study 2000. J Geophysical Res. 108, 4508, doi:10.1029/2002JD003333, 2003.

Karl, T., Christian, T., Yokelson, R., Artaxo, P., Hao W. and Guenther, A.: The Tropical Forest and Fire Emissions Experiment: method evaluation of volatile organic compound emissions measured by PTR-MS, FTIR, and GC from tropical biomass burning. Atmos. Chem. Phys., 7, 5883–5897, 2007.

Lindinger, W., Hansel, A. and Jordan, A.: On-line monitoring of volatile organic compounds at pptv levels by means of Proton-Transfer-Reaction Mass Spectrometry (PTR-MS) Medical applications, food control and environmental research. International Journal of Mass Spectrometry and Ion Processes. 173, 191-241, 1998.

Rinne, J., Ruuskanen, T.M., Reissell, A., Taipale, R., Hakola, H. and Kulmala, M.: On-line PTR-MS measurements of atmospheric concentrations of volatile organic compounds in a European boreal forest ecosystem. Boreal Environment Research. 10, 425-436, 2005.

Ulbrich, I. M., Canagaratna, M. R., Zhang, Q., Worsnop, D. R., and Jimenez, J. L.: Interpretation of organic components from Positive Matrix Factorization of aerosol mass spectrometric data, Atmos. Chem. Phys., 9, 2891–2918, 2009.